Challenge Journal of

CONCRETE RESEARCH LETTERS

Vol.9 No.3 (2018)

acidic environment acoustic emission compressive strength concrete corrosion cracking deformation characteristics ductility durability energy absorption ferrocement fly ash mechanical properties palm oil fuel ash reinforced concrete self-compacting concrete serviceability load silica fume steel mesh strength strengthening water a[illegible]ion

ISSN 2548-0928

TULPAR ACADEMIC PUBLISHING

Challenge Journal of Concrete Research Letters

E-mail: *cjcrl@challengejournal.com*

Web page: *cjcrl.challengejournal.com*

TULPAR Academic Publishing
www.tulparpublishing.com

Challenge Journal of Concrete Research Letters

CONTENTS

Research Articles

Challenge Journal of Concrete Research Letters

Research Article

Properties of sand cement brick containing ground palm oil fuel ash as fine aggregate replacement

Khairunisa Muthusamy [a,*], Muhammad Azreen Ibrahim [a], Nor Hazurina Othman [b], Ahmed Mokhtar Albshir Budiea [c], Saffuan Wan Ahmad [a]

[a] *Faculty of Civil Engineering and Earth Resources, Universiti Malaysia Pahang, Lebuhraya Tun Razak, 26300 Gambang, Kuantan, Malaysia*
[b] *Faculty of Civil and Environmental Engineering, Universiti Tun Hussien Onn Malaysia, 86400 Parit Raja, Batu Pahat, Malaysia*
[c] *Perunding Teknik Padu, Lot 192-B, Wisma Qistina, Pusat Perniagaan Bandar Baru Beris Kubur Besar, Bachok, Malaysia*

ABSTRACT

The prosperous palm oil industry continues to generate increasing amount of palm oil fuel ash which disposed as environmental polluting waste. Thus, research was conducted to investigate the effect of ground palm oil fuel ash as partial fine aggregate replacement towards properties of sand cement brick. Series of mixes were prepared with 0%, 5%, 10%, 15%, 20% and 25% ground palm oil fuel ash partially substituting the river sand. Two types of curing methods were applied namely water and air curing. The bricks were subjected to compressive strength, flexural strength and water absorption test at 28 days. The results show that utilization of 15% ground palm oil fuel ash as fine aggregate replacement increases the brick strength. The pozzolanic reaction and filler effect of the finely ground ash makes the concrete internal structure denser resulting in strength enhancement. The use of ground palm oil fuel ash in brick production would reduce amount of palm oil waste disposed, save the use of land for dumping purpose and decrease quantity of river sand mined.

ARTICLE INFO

Article history:
Received 26 July 2018
Accepted 25 August 2018

Keywords:
Ground palm oil fuel ash
Fine aggregate replacement
Sand cement brick
Air curing
Material properties

1. Introduction

In Malaysia, both construction trade and palm oil industry contribute to the development of the country. The increasing population calls for more construction of facilities. Sand cement brick is one of the materials which widely used in building construction. The increasing brick production also raises the sand mined from the river. Extreme river sand mining tends to destroy the river vegetation and disturbs the habitats of fauna. Finally if the situation continues, it causes reduction of the aquatic life population threatened to extinction. The adverse effect of river sand mining towards the environment and topographical of river is pointed out by previous researchers, Sathiparan and De Zoysa (2018). Thus, exploration of alternative material to be used as fine aggregate replacement is one of solution to reduce high dependency on natural river sand supply. Converting the available local waste material to be used as fine aggregate for construction material production would be benefitting the environment and community surrounding.

At the same time, palm oil industry which continuously expanding generates plentiful waste over the year. The industry which begins with a small commercial plantation in Kuala Selangor in 1917 has flourished immensely reaching to a total of 5.81 million hectares plantation area all over the country in 2017 (Khusairi et al, 2018). Along with the increasing production of palm oil, this industry also generates a large amount of by-product which disposed as environmental polluting waste. One of the wastes is palm oil fuel ash (POFA), a light ash particles formed during the combustion of palm oil fibre, empty fruit bunch and shell for energy generation at the mill. In practice, this waste is thrown at allocated dumping site within the palm oil mill area and it pollutes the environment. The environmental pollution due to dumping of this waste was highlighted by previous researchers Aprianti (2017) and Muthusamy et al (2018). Continuous

* *Corresponding author*. E-mail address: khairunisa@ump.edu.my (K. Muthusamy)
ISSN: 2548-0928 / DOI: https://doi.org/10.20528/cjcrl.2018.03.001

disposal of this material would lead to accumulation of the waste consuming larger dumping area and more pollution which is unhealthy for surrounding community.

Realizing the need for cleaner and sustainable environment, many researchers namely Awal and Hussin (1997), Chinaprasirt et al. (2007), Ismail et al. (2010), Zeyad et al. (2013), Megat Johari et al. (2012), Awal and Shehu (2015), Muthusamy et al. (2015), Ul Islam et al. (2016), Salami et al. (2018) Al Subari et al (2018) successfully integrated POFA as partial cement replacement owing to its pozzolanic properties and produces concrete with enhanced properties. There are few researchers Mat Yahaya et al (2016), Wan Ahmad et al (2017) used POFA as fine aggregate replacement in concrete production. However, very limited research is available on the performance of sand cement brick produced using POFA as mixing ingredient. Thus, the present study investigates the effect of ground POFA as partial fine aggregate replacement on properties of sand cement brick.

2. Experimental Details

The brick composition mainly consists of three types of materials namely cement, water and local river sand. Ordinary Portland cement (OPC) from a single source was used throughout the experimental work. Tap water was used for mixing and curing purposes. Palm oil fuel ash (POFA) was obtained from a palm oil mill located in East Coast of Peninsula Malaysia. POFA was collected from an open dumping area at mill as illustrated in Fig. 1. Then, it was oven dried for 24 hours. After ensuring the ash is free from foreign particles, it was ground to be fine to enhance it pozzolanic effect before keeping it in a closed container.

Fig. 1. Palm oil fuel ash disposal space at the mill.

Six types of brick mixes with the dimension size of 210 x 100 x 65 mm were prepared. The control brick specimen was prepared with 0% palm oil fuel ash (POFA). The rest four mixes of brick were prepared by replacing the percentages of POFA from 5%, 10%, 15%, 20%, and 25% by the weight of the sand. The brick mixing work were conducted using a mixing machine to ensure a uniform mix. Then, it is filled in the mould, compacted and left overnight before demoulded the next day. All specimens were subjected to air curing as shown in Fig. 2. All of the specimens were tested for compressive strength, flexural strength and water absorption test. All tests were conducted in accordance to ASTM C55 (2017).

Fig. 2. Sand cement bricks subjected to air curing.

3. Results and Discussion

3.1. Compressive and flexural strength

Figs. 3 and 4 show the compressive strength and flexural strength result of specimens subjected to different curing. The strength performance of all specimens continues to increase as the curing age become longer. This is attributed to the high humidity condition of the tropical weather which allows extended time for water retention in the brick in contrast to exposure in dry weather which would speed up water evaporation. The moist condition enables the occurrence of chemical reaction for C-S-H gel production which is vital for strength enhancement of the brick. Similar observation has been reported by previous researcher Shafigh et al. (2013) who used other types of pozzolanic material as mineral admixture in lightweight concrete. Looking at the effect of ash content, it is observed that replacement up to 20% POFA successfully enhances the brick strength. However, the highest strength performing brick is the one produced with 15% POFA. Generally, strength of the specimens increases due to the pozzolanic reaction and the ability of fine ground POFA to fill the voids inside the specimen making it more compact and stronger. However incorporation of 25% POFA causes reduction in the brick strength. The use of POFA in higher amount reduces the workability of mix and makes it difficult to be compacted which produces brick with higher number of voids and lower strength. Conclusively, the use of ground palm oil fuel ash at suitable percentage improves the strength of sand cement brick.

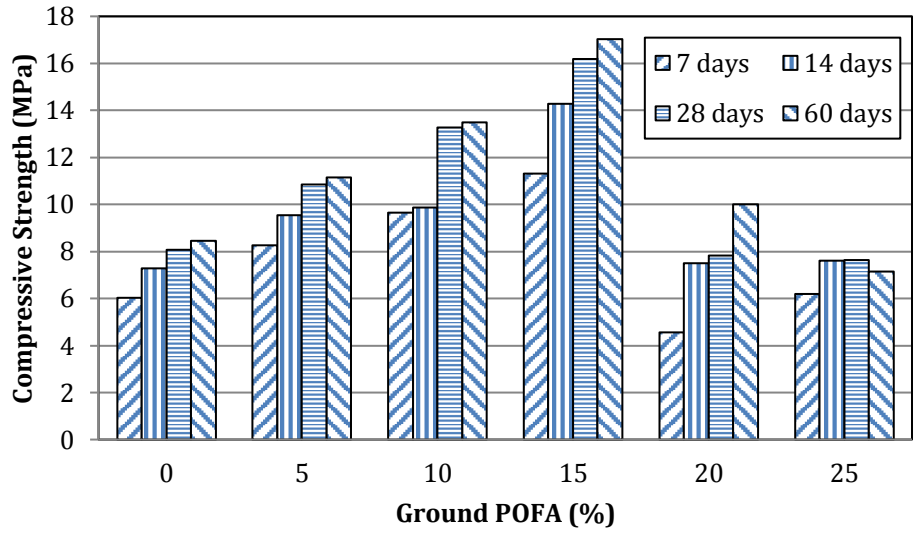

Fig. 3. Compressive strength results of brick with ground POFA content up to 60 days.

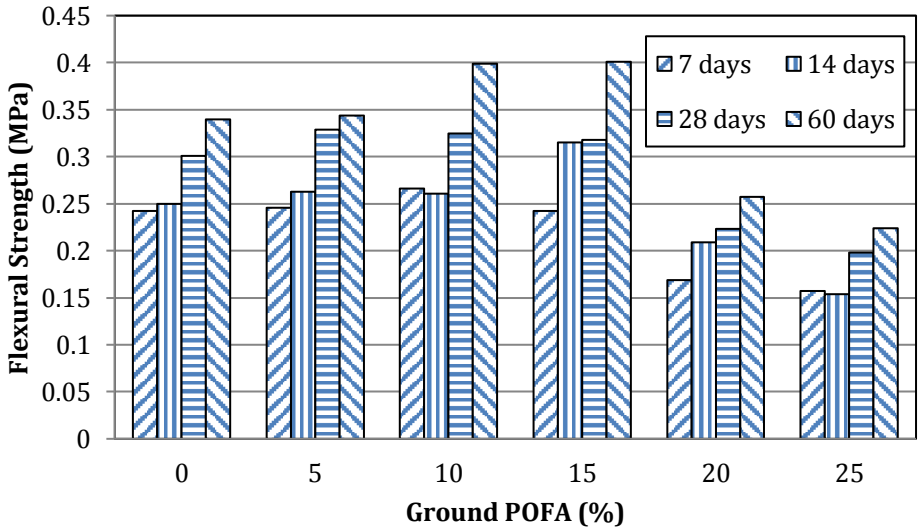

Fig. 4. Flexural strength result of brick with ground POFA content up to 60 days.

3.2. Water absorption

Fig. 5 illustrates the water absorption of brick containing various ground POFA content. Evidently, use of POFA affects the water absorption of the brick. The water absorption of the bricks reduces when POFA is integrated up to 15%. This is believed to be due to the function of the ground ash in forming a denser internal structure of the brick. The positive role of fine POFA in terms of voids filling capability has been pointed by previous researcher Abdul Awal, (1998). However, use of higher content of POFA of 20 and 25% dramatically increases the water absorption. Therefore, it is recommended that the use of POFA as fine aggregate replacement in sand cement brick should be limited not more that 15%.

4. Conclusions

The following conclusions can be drawn from the results:

- With regard to compressive strength and flexural strength, water cured brick containing 15% ground palm oil fuel ash as partial fine aggregate replacement recorded the highest strength of all specimens.
- Utilization of ground POFA up to 15% contribute in reduction of the brick water absorption percentage.
- The thermal conductivity and fire resistance performance of sand cement brick containing ground POFA is among the properties that remains to be explored in future research.
- The present research founds that ground POFA could be a prospective material as a partial sand replacement material for sand cement brick production.

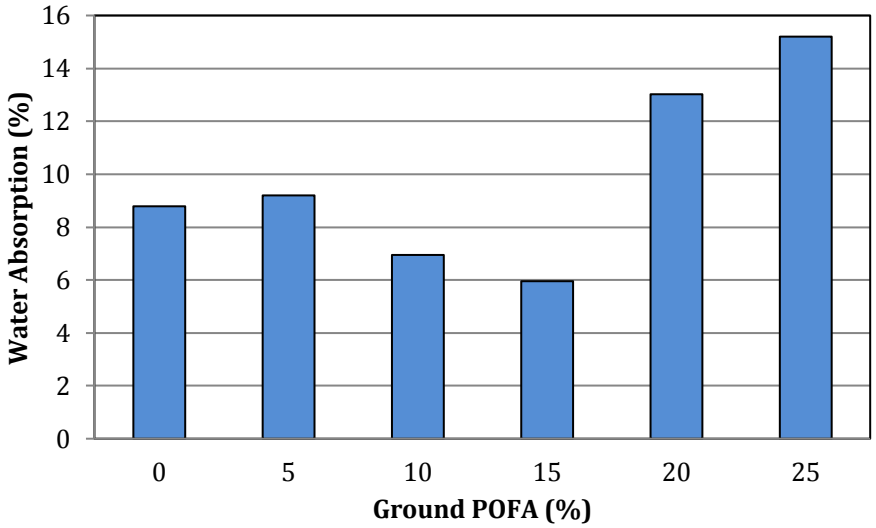

Fig. 5. Water absorption result with ground POFA content at 28 days.

Acknowledgements

The works are funded by research grant (RDU 170339) sponsored by Universiti Malaysia Pahang.

REFERENCES

Abdul Awal ASM (1998). A Study of Strength and Durability Performances of Concrete Containing Palm Oil Fuel Ash. *Ph.D thesis*, Universiti Teknologi Malaysia, Malaysia.

Abdul Awal ASM, Hussin MW (1997). The effectiveness of palm oil fuel ash in preventing expansion due to alkali silica reaction. *Cement and Concrete Composites*, 19(4), 367-372.

Abdul Awal ASM, Shehu I (2015). Performance evaluation of concrete containing high volume palm oil fuel ash exposed to elevated temperature. *Journal of Construction and Building Materials*, 76, 214-220.

Alsubari B, Shafigh P, Ibrahim Z, Alnahhal MF, Jumaat MZ (2018). Properties of eco-friendly self-compacting concrete containing modified treated palm oil fuel ash. *Construction and Building Materials*, 158(15), 742-754.

Aprianti E (2017). A huge number of artificial waste material can be supplementary cementitious material (SCM) for concrete production – a review part II. *Journal of Cleaner Production*, 142(4), 4178-4194.

ASTM C55 (2017). Standard specification for concrete building brick. ASTM Internationals, West Conshohocken, Philadelphia.

Chindaprasirt P, Homwuttiwong, S and Jaturapittakul C (2007). Strength and water permeability of concrete containing palm oil fuel ash and rice husk-bark ash. *Construction and Building Materials*, 21, 1492–1499.

Ismail MA, Budiea AMA, Hussin MW, Muthusamy K, (2010). Effect of POFA fineness on high strength POFA concrete. *Indian Concrete Journal*, 84, 21-27.

Khusairi A, Loh SK, Azman I, Hishamuddin E, Ong-Abdullah M, Mohd Noor Izzuddin ZB, Razmah G, Sundram S, Ahmad Parveez GK (2018). Oil palm economic performance in Malaysia and R & D progress in 2017. *Journal of Oil Palm Research*, 30(2), 163–195.

Mat Yahaya F, Muthusamy K, Hussin M W (2016). Long term investigation on sulphate resistance of aerated concrete containing palm oil fuel ash. *ARPN Journal of Engineering and Applied Sciences*, 11(4), 2406-2411.

Megat Johari MA, Zeyad AM, Muhammad Bunnori N, Ariffin KS (2012). Engineering and transport properties of high-strength green concrete containing high volume of ultrafine palm oil fuel ash. *Construction and Building Materials*, 30, 281–288.

Muthusamy K, Zamri NA, Kusbiantoro A (2018). Effect of palm oil fuel ash on compressive strength of palm oil boiler stone lightweight aggregate concrete. *IOP Conference Series: Materials Science and Engineering*, 342, 1-5

Muthusamy K, Zamri NA, Zubir MA, Kusbiantoro A, Wan Ahmad S, (2015). Effect of mixing ingredient on compressive strength of oil palm shell lightweight aggregate concrete containing palm oil fuel ash. *Procedia Engineering*, 125, 804-810.

Salami BA, Megat Johari MA, Ahmad ZA, Maslehuddin M (2017). Performance of palm oil fuel ash-based engineered alkaline-activated cementitious composite (POFA-EACC) mortar in sulfate environment. *Construction and Building Materials*, 131, 229-244.

Sathiparan N, De Zoysa HTSM (2018). The effects of using agricultural waste as partial substitute for sand in cement blocks. *Journal of Building Engineering*, 19, 216-227.

Shafigh, P, Mohd Zamin J, Hilmi M, Alengaram UJ (2013). Oil palm shell lightweight concrete containing high volume ground granulated blast furnace slag. *Construction and Building Materials*, 40, 231-238.

Ul Islam MM, Mo KH, Alengaram UJ, Jumaat MZ (2016). Durability properties of sustainable concrete containing high volume palm oil waste materials. *Journal of Cleaner Production*, 137, 167–177.

Wan Ahmad S, Muthusamy K, Hashim H, Yaacob MA (2017). Properties of concrete containing unground palm oil fuel ash as partial sand replacement. *Applied Mechanics and Materials*, 854, 278-283.

Zeyad AM, Megat Johari MA, Muhammad Bunnori N, Ariffin K S, Altwair N M (2013). Characteristics of treated palm oil fuel ash and its effects on properties of high strength Concrete. *Advanced Material Research*, 626, 152-156.

Challenge Journal of Concrete Research Letters

Research Article

Concrete strength prediction using artificial neural network and genetic programming

Preeti Kulkarni, Shreenivas N. Londhe *

Department of Civil Engineering, Vishwakarma Institute of Information Technology, Pune 411048, India

ABSTRACT

Concrete is a highly complex composite construction material and modeling using computing tools to predict concrete strength is a difficult task. In this work an effort is made to predict compressive strength of concrete after 28 days of curing, using Artificial Neural Network (ANN) and Genetic programming (GP). The data for analysis mainly consists of mix design parameters of concrete, coefficient of soft sand and maximum size of aggregates as input parameters. ANN yields trained weights and biases as the final model which sometime may impediment in its application at operational level. GP on other hand yields an equation as its output making its plausible tool for operational use. Comparison of the prediction results displays the result the model accuracy of both ANN and GP as satisfactory, giving GP a working advantage owing to its output in an equation form. A knowledge extraction technique used with the weights and biases of ANN model to understand the most influencing parameters to predict the 28 day strength of concrete, promises to prove ANN as grey box rather than a black box. GP models, in form of explicit equations, show the influencing parameters with reference to the presence of the relevant parameters in the equations.

ARTICLE INFO

Article history:
Received 2 June 2018
Revised 6 September 2018
Accepted 11 September 2018

Keywords:
Artificial neural network
Genetic programming
Concrete
Compressive strength

1. Introduction

Concrete is a material with a mix of main constituents Cement, Aggregates and water. The properties of concrete depend on various parameters including the non-homogeneous nature of their components, different properties of various materials used and also the contradictory effects of some materials on the overall concrete performance. The strength of concrete are thus functions of relative magnitudes of these various concrete mixes. To ascertain the strength of concrete with use of these materials need extensive testing and time (28 day being standard) (Shetty, 2005). A need thus arises to use soft computing tools in prediction of concrete properties with acceptable performance which can reduce the consumption of materials and save time. Development of models using relevant soft computing tools can also help in designing the appropriate mix proportions for a required grade of concrete thus leading towards economic utilization of materials. Many researchers earlier have made an attempt to predict strength of concrete and other properties using techniques like Artificial Neural Network (ANN) (Mukherjee and Sudip, 1997; Meltem et al., 2008; Ni and Wang, 2000; Ahmet et al., 2006; Gorphade et al., 2014), Genetic Programming (GP) (Gandomia et al. 2014; Sarıdemir, 2010), Fuzzy systems etc. (Khademi et al. 2016; Khademi et al. 2017; Behfarnia and Khademi, 2017). ANN has been used in predicting the stress–strain behavior of concrete and ANN understands the relationship and the performance was superior to the existing mathematical models (Mukherjee and Sudip, 1997). ANN, Multiple Linear Regression (MLR) and Abram's law were used to predict concrete strength with input parameters as concrete mix proportions, Fresh Density and 7-days compressive strength, showing that MLR models are better in strength prediction of concrete than ANN models for models which include only the constituent materials and fresh concrete data and with early strength data in two models better prediction of strength by ANN models was seen (Meltem et al., 2008). ANN

* *Corresponding author*. Tel.: +20-942-2037789 ; E-mail address: shreenivas.londhe@viit.ac.in (S. N. Londhe)
ISSN: 2548-0928 / DOI: https://doi.org/10.20528/cjcrl.2018.03.002

technique was used to predict the compressive strength of concrete with input parameters as water cement ratio, grade of cement, water dosage etc. The study shows that strength of concrete is direct proportion to the dosage of cement. Slight influence of sand to aggregate ratio on strength can be seen. Rules obtained by ANN models are consistent with those by laboratory work and exhibit good performance (Ni and Wang 2000). The applicability of ANN to predict the CS and slump of high strength concrete can be seen with ANN model with input parameters as water to binder ratio, fine aggregate ratio, water content, fly ash content etc. ANN shows reasonably good predictions with R^2 values as 99.8% and 99.25% in training set and 99.93% and 99.34% in test set for CS and slump, respectively (Ahmet et al., 2006). Prediction of the strength characteristics and workability and Young's modulus of High performance concrete was done using Genetic Algorithm based neural network models with an accuracy of about 95% (Gorphade et al. 2014). Linear genetic programming (LGP) technique was used in predicting strength capacity of Reinforced Concrete (RC) beams. The proposed design equation displays reliable estimations of the strength capacity of RC beams without stirrups and is also capable of capturing the underlaying physis of the same. The LGP model displays better outcomes than the existing building codes (Gandomia et al. 2014). Saridemir (2010) developed two models using gene expression programming (GEP) approach for predicting compressive strength of concretes with rice husk ash at the various ages from 1 to 90 days. The models in results for the testing and validation stages shows a good generalization capacity and low error values (Sarıdemir, 2010). Fuzzy Interference system and Regression analysis was also used to predict strength of concrete, displacement determination of reinforced building (Khademi et al., 2016; Khademi et al., 2017; Behfarnia and Khademi, 2017). Literature review thus signifies that ANN and GP are used in predicting strength but the use of properties of materials as additional input parameters and knowledge extraction from the weights and biases of ANN has been seldom done and discussed. The aim of the present study is thus to develop models predicting strength of concrete at 28 day with various input parameters, using soft computing techniques i.e. Artificial Neural Networks (ANN) and Genetic Programming (GP) and compare the performance of the same. ANN displays the output in form of weights and biases and Genetic Programming in form of equations. Knowledge extraction technique from ANN is used further and the influence of input parameter on output is studied and compared with the domain knowledge. Genetic Programming equations developed are significant in understanding the influence of input parameters.

In the further sections of the current work, basic concepts of artificial neural network, Knowledge extraction and Genetic Programming are discussed, followed by details of data used in the current study. Model development methodology is then presented followed by results and discussion. The current work ends with a conclusion.

2. Modeling Techniques

2.1. Artificial neural network (ANN)

ANN is a soft computing technique is inspired by the biological network of human brain. Similar to working of biological network, Artificial Neural Network consists of basic three layers viz. input layer, hidden layer and the output layer. The input and output layers are connected to hidden layer by weights, biases and transfer functions. The error is computed with the difference between output and the target. This error is propagated back and the weight and biases are adjusted using optimization technique to minimize the error. The error optimization process is repeated for number of iterations till the desired accuracy is achieved. Once the desired accuracy is achieved, validation of the developed model is done on unseen data. Readers are referred to for details of ANN to Londhe et al. (2009).

2.2. Knowledge extraction from ANN

ANN is said to be a performing tool, however little is known about what's happening inside it which can be slightly seen through Hinton diagram, and thus the performance of ANN is questioned many a times (Deshpande et al., 2014). It is difficult to monitor the relation between input and output parameters as the knowledge may not be extracted from the neural network and thus knowledge extraction is important. Rule extraction has three phases: decomposition, pedagogical, and eclectic (Kahramanli and Allahverdi, 2001). To obtain the influence of each input variable on the output of a trained feed-forward multilayer perceptron to estimate monthly runoff, Garson's model was used (Phukoetphim et al., 2014). However, it was seen that the magnitude and the nature of the contribution of the input parameters was not correctly displayed by Garson's algorithm. The models were developed with input parameters as maximum humidity, sunshine duration, maximum and minimum temperature and wind speed and pan evaporation (mm/day) as the output. Thus showing that this method of knowledge extraction is not applicable at least for evaporation modelling using ANN (Londhe and Shah, 2016). Thus to extract the knowledge locked up in the network, a new method was formulated by the authors. The new method suggests an algebraic sum of the influences of the inputs, which are obtained at two stages of the neural network programming. Hence, the method takes into consideration the signs of the weights extracted from the neural networks and thus would be able to give not only the magnitude but also nature of the influence of each input on the output. The procedure of obtaining the influence of inputs at both stages of programming and their summation is given in Appendix A (Londhe and Shah, 2016).

2.3. Genetic programming (GP)

Genetic programming (GP) was inspired by biological evolution is a machine learning technique and based on

principle of survival of fittest, to compute computer programs/ equations that solve a problem. It uses the principle of Darwinian natural selection to evolve a program. GP operates on parse trees to approximate the equation or computer program that best displays the output to input variables. To transfer one population of individuals into other one natural genetic operations like reproduction, mutation and cross-over are utilized in GP. The flowchart of GP is given in Fig. 1 below (Koza, 1992; Londhe and Dixit, 2012).

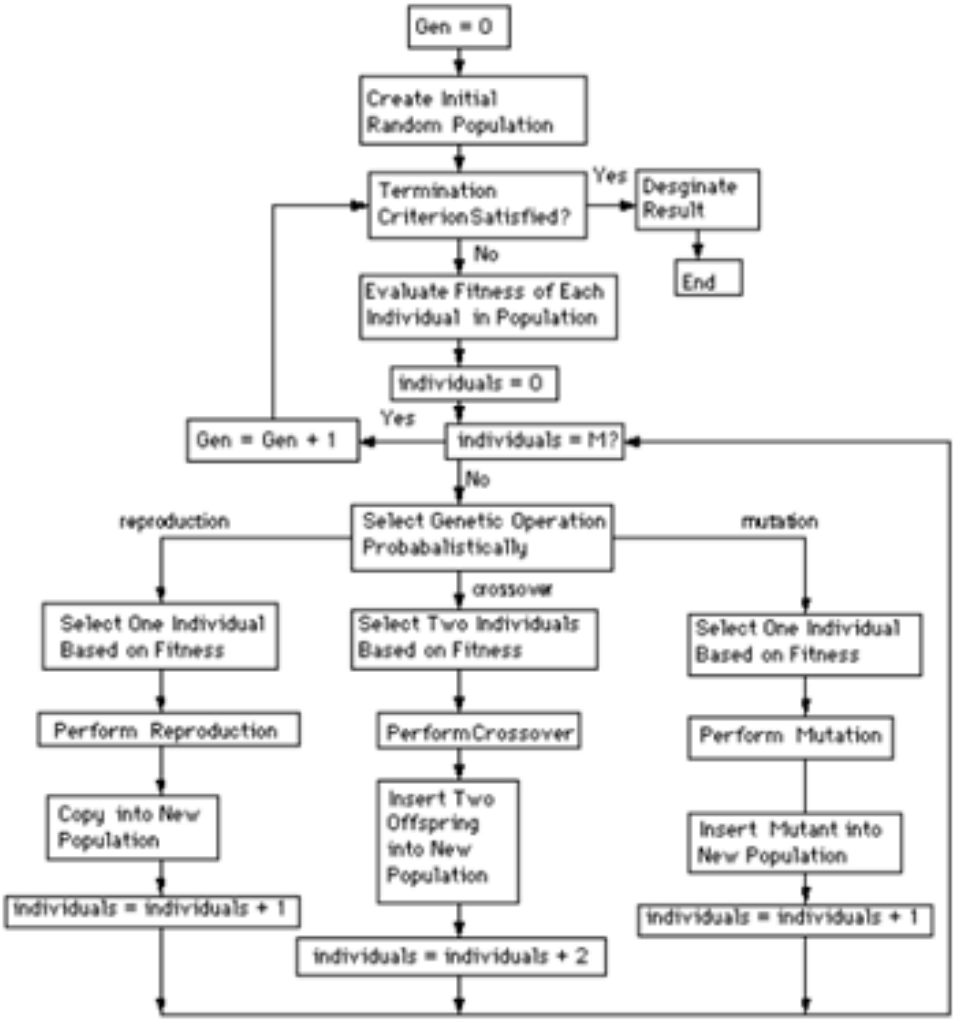

Fig. 1. Flowchart of genetic programming.

For details of the same readers are referred to Londhe and Dixit (2012). The three genetic operations are as follows:

Reproduction: An individual is chosen from the first population and is replicated exactly into the subsequent generation and the program which does not perform are removed. Fitness measure, selection, rank selection and tournament selection are few methods of selection from which individual are duplicated.

Cross over: Two parent results are selected and parts of their sub-tree are exchanged such that each function holds the property 'closure' (each tree member can transform all possible argument values).

Mutation: it provides diversity to the population. The mutation operator selects a node in the parse tree and replaces the branch at that node by a randomly generated branch. Perspective to portray GP as far as the structures that experiences adaptations are:

1. Initial structure generation
2. Fitness measure test which assesses the structure
3. Operations which change the structure
4. The state (memory) of the framework at each stage
5. The system for terminating the process

The system for designating the output and parameters that control the process. Linear representation of computer programming is used in linear genetic programming (LGP). Each individual (Program) in LGP is represented by a variable-length sequence of simple C language instructions, which operate on the registers or constants from predefined sets. The function set of the system can be composed of arithmetic operations (+, - , X, /), conditional branches, and function calls (f {x, xn, sqrt, ex, sin, cos, tan, log, ln}). The readers are further referred to Phukoetphim et al. (2014) and Londhe and Dixit (2012).

3. Modeling Data

A total of 149 data was collected from literature, which consists of testing the compressive strength of cylindrical samples with a diameter of 15 cm and a height of 30 cm are used (Kumar and Kumar, 2015; Oner and Akyuz, 2007; Lee et al., 2006). In addition, parameters such as the amount of 3/4 sand, 3/8 sand, cement, silt in kilograms, maximum sand size in millimeter, coefficient of fine sand, and water-cement ratio are used to determine the 28 day strength of concrete. The characteristics of used data have been illustrated in Table 1. The average mutual information (AMI) i.e. nonlinear relation of each parameter with the output and correlation coefficient of input parameter with output is also shown in Table 1 (Bhattacharya and Solomatine, 2005). The sample data used in the work is as shown in Table 2 below.

Table 1. Characteristics of Input and output parameters.

Sr. No	Input Parameters	Range of Values (min-max)	AMI	Correlation coefficient	Mean
1	Cement Content (C) kg	243-549	5.119	0.725	385.550
2	Water cement ratio (WC)	0.240-0.500	2.637	-0.856	0.430
3	Maximum size of Sand (MA) cm	5.120-50	3.247	0.058	23.890
4	Gravel (SA) kg	559-1050	5.542	-0.495	779.130
5	Sand 3/8 (G1) kg	303-523	4.323	0.085	427.050
6	Sand ¾ (G2) kg	365-693	4.358	0.042	563.310
7	Coefficient of soft sand (FM)	2.400-9.200	2.423	-0.017	3.270
	Output Parameter in kg/cm^2				
1	28 day compressive strength of concrete kg/cm^2 (ST)	173 -394	-		279.270

Table 2. Sample of data used in the work.

C (kg)	WC	MA (cm)	Gravel (SA) (kg)	Sand 3/8 kg G1	Sand ¾ kg G2	Coefficient of soft sand FM	28 day compressive strength of concrete kg/cm^2 ST
413	0.4	3.75	617	647	488	3	300
431	0.42	2.5	740	584	439	3.1	352
406	0.56	0.95	863	437	330	2.6	235
371	0.41	5	772	656	495	3.2	319
348	0.48	3.75	794	629	474	3.4	318
354	0.48	5	682	693	523	2.7	331
436	0.41	3.75	648	647	488	2.6	363
494	0.42	1.9	620	584	439	2.8	394
323	0.48	5	812	656	495	3.1	322
420	0.4	1.9	675	583	440	2.5	282

4. Methodology for Model Development

Four different models were developed in the current study using ANN and GP with common output as 28th day compressive strength of cylindrical concrete samples. The abbreviations used for the models developed are shown in Table 3. ANN1 and GP1 was developed with basic mix design parameters as Sand 3/8 (G1) in kg, Sand 3/4 (G2) in kg, Cement content (C) in kg, Gravel (SA) in kg and water cement ratio (WC) ratio as input parameters. ANN2 and GP2 were the new set of models developed with additional input parameters of coefficient of soft sand (FM) and maximum size of aggregate (MA) in cm as in ANN1 and GP1.

ANN models with 3 layers i.e. input, hidden and output layer were developed using MATLAB Neural Network toolbox. Development of ANN model was done with three layered "Feed forward Back propagation" network to predict the 28 day compressive strength of concrete and was trained till a very low performance error (mean squared error) was achieved. In order to determine the number of neurons in the hidden layer, the following experimental formula (Eq. (1)) was used (Bowden et al., 2005).

$$NH \leq 2N1 + 1\,, \tag{1}$$

where NH is the maximum number of nodes in the hidden layer and N1 is the number of inputs. With regard to the fact that the number of obtained effective inputs is equal to 7, maximum number of nodes in the hidden layer is 15 (NH ≤ 15). All the networks were trained using Levernberg-Marquardt algorithm with 'log-sigmoid 'transfer functions in between first (input) and second (hidden) layer and 'linear' transfer function between the second and third layer (output). The data was normalized between 0 and 1. For developing equation using GP, GPKERNEL software was used. The various parameters which were decided for the same are as follows:
Population size: 500
Number of children to be produced: 500
Operators: exp(x), pow(x, 2), sqrt(x), (x + y), (x - y), (x * y), (x / y), pow(x, y).
Objective functions: Coefficient of determination and Root mean squared error
Maximum Subtree Mutation Size=15
Crossover rate=0.4

The data division was done as follows: 70% of data was used for training and 30% for testing which remains same for model development using ANN and GP techniques. The model's performance were assessed by statistical measures Normalized root mean squared error (NRMSE), correlation coefficient (R), Nash-Sutcliffe Efficiency (E) and Average absolute error (AARE) (Legates and McCabe, 1999; Dias and Pooliyadda, 2001).

Table 3. Abbreviations for the models developed using ANN and GP.

Sr. No	Input Parameters	ANN Model	GP Model
1	G1, G2, C, SA, WC	ANN1	GP1
2	FM, G1, G2, C, SA, MA, WC	ANN2	GP2

5. Results and Discussion

The current study makes an attempt to explore the applicability of models developed using ANN and GP for the prediction of 28 day concrete compressive strength with input parameters as: Sand 3/8 (G1) in kg, Sand 3/4 (G2) in kg, Cement content (C) in kg, Gravel (SA) in kg and water cement ratio (WC) ratio, coefficient of soft sand (FM) and maximum size of aggregate (MA).This section presents the comparative investigation of results obtained from ANN and GP approaches and quantitative assessment of the models. An investigation into understanding the influential parameters in predicting strength of concrete is done in the later stage. Mix design of concrete typically consists of calculation of proportions of materials used in concrete per cubic meter (Shetty, 2005). With the same view, ANN1 and GP1 model was developed with mix proportions of concrete as input parameters as shown in Table 4. The developed models were validated with 30% of testing data using error measures as shown in Table 4 below.

Table 4. Details and results of models developed.

Sr. No	Input Parameters	Model	Architecture	R	NRMSE	AARE	E
1	G1, G2, C, SA, WC	ANN1	5:11:1	0.937	0.078	6.625	0.852
2	G1, G2, C, SA, WC	GP1	-	0.917	0.147	12.816	0.478
3	FM, G1, G2, C, SA, MA, WC	ANN2	7:15:1	0.941	0.078	6.674	0.854
4	FM, G1, G2, C, SA, MA, WC	GP2	-	0.894	0.096	7.627	0.780

Table 4 shows that model ANN1 developed with mix design parameters as input parameters and architecture of 5:11:1, shows a better performance, with correlation coefficient R as 0.936, than GP1 model with same input parameters and R value as 0.917. Lower values of AARE and NRMSE and higher values of R and E for ANN1 indicate that the model can predict compressive strength of the mixes with high reliability as compared to GP1. ANN predicts the output better than GP in the current study but showcases a limitation of simplified equation which can be computed easily. Genetic programming (GP) on the other hand can provide an equation which can be used by a general user. The GP1 developed is as shown in Eq. (2):

$$ST = \left(\sqrt{(G_2+C)\sqrt{\left(C+\left((SA+C)\sqrt{\sqrt{G_1^2}}\right)\right)}+(C+(-4.3+C))}-\left(\left(C+\sqrt{(C+SA)+WC}\right)+(C+G_2)^{WC}\right)\right)-(G_1^{WC}) \quad . \quad (2)$$

The next set of models developed were ANN2 and GP2 with mix design parameters and coefficient of sand (FM) and Maximum size of aggregate (MA) as additional input parameters. Coefficient of soft sand i.e. fineness modulus of sand has an impact over the strength of concrete. An increase in fineness modulus of sand implies the increase coarsens of sand which can result further in decrease strength of concrete for given conditions (Shetty, 2005). Similarly maximum size of aggregate needs to be restricted to gain the required strength of concrete. With increase in size of aggregate (after a certain limit) increases the amount of voids in the concrete

mix which can further lead to decrease in strength of concrete (Shetty, 2005). ANN2 with architecture of 7:15:1 displays a good performance with correlation coefficient as 0.941. The performance is also validated with other error measures as shown in Table 4.

Weights and bias developed for ANN2 is as shown in Appendix B.

The equation developed by GP2 is:

$$ST = \frac{\sqrt{\left(\left(\sqrt{G1}\,\frac{MA^2}{\sqrt{SA}}\right)^2\right) + \left(\sqrt{\sqrt{C}\cdot C}\right)} \cdot \sqrt{\sqrt{\sqrt{\sqrt{FM}\cdot G2}+G2}}}{\sqrt{WC}} \quad . \qquad (3)$$

Eq. (3) developed using GP for GP2 shows the presence of all input parameters considered in the model and displays a satisfactory performance. Thus it can be said that ANN and GP models can be developed with acceptable performance when FM and MA are known. The table 4 below shows the sample of predictions done by developed ANN and GP model.

Thus the above study shows that ANN technique predicts 28 day strength of cylindrical concrete specimens better than GP technique in both the models. ANN builds an approximate function that matches a list of inputs to the desired outputs. In the process it adjusts the weights and biases to reach a predefined goal. This process makes ANN flexible and increases its performance as compared to GP. GP on other hand is based on evolutionary approach technique in which it does not involve any transfer function and evolves generations of 'offspring' based on the 'fitness criteria' and genetic operations. GP approach works with the concept of disregarding input parameters that do not that contribute beneficially to the model and thus based solely on 'fitness' criteria. In the process of building programs (through processes of mutation, crossover and reproduction), GP shows predictions which are slightly over predicted as compared to ANN (Refer Fig. 3) and thus GP shows a performance less as compared to ANN. Addition of material properties as Soft coefficient of sand and maximum size of aggregates as input parameters in developing ANN and GP models helps in predicting concrete strength is slightly better than the models with input parameters as mix design proportions. Though GP2 shows a reduction in R value as compared to GP1, the reduction is not very significant. Thus it can be said that inclusion of material properties as input parameters in development of models is beneficial for to capture the underlying phenomenon of the subject in detail. Figs. 2 and 3 show the scatter plot for ANN1 and GP2 respectively. The scatter plots for ANN1, ANN2 and GP2 do not exhibit an obvious under or over prediction. The trend of predicting concrete strength by GP1 is as shown in Fig. 4. It also shows ANN predicted values to be in tune with the Observed values but slight over prediction of strength in GP.

Table 5. Sample predictions and percentage errors for each model developed.

Observed Values of 28 day strength in kg/cm²	Predictions							
	ANN1	Error (%)	GP1	Error (%)	ANN2	Error (%)	GP2	Error (%)
226	246.287	8.237	283.966	20.413	249.273	9.336	243.822	7.309
211	209.299	-0.813	226.662	6.910	225.757	6.537	193.845	-8.850
279	318.718	12.462	332.281	16.035	325.924	14.397	284.525	1.942
321	295.755	-8.536	324.072	0.948	303.561	-5.745	272.882	-17.633
326	306.208	-6.464	325.658	-0.105	311.104	-4.788	280.927	-16.045
285	281.224	-1.343	329.124	13.407	277.351	-2.758	307.824	7.415
249	239.717	-3.873	272.051	8.473	239.819	-3.828	233.114	-6.815
347	355.604	2.419	358.385	3.177	354.858	2.214	341.444	-1.627
343	348.216	1.498	355.938	3.635	344.578	0.458	327.756	-4.651
231	244.655	5.581	282.097	18.113	242.194	4.622	237.336	2.670

Thus the above study shows that ANN technique predicts 28 day strength of cylindrical concrete specimens better than GP technique in both the models. ANN builds an approximate function that matches a list of inputs to the desired outputs. In the process it adjusts the weights and biases to reach a predefined goal. This process makes ANN flexible and increases its performance as compared to GP. GP on other hand is based on evolutionary approach technique in which it does not involve any transfer function and evolves generations of 'offspring' based on the 'fitness criteria' and genetic operations. GP approach works with the concept of disregarding input parameters that do not that contribute beneficially to the model and thus based solely on 'fitness' criteria. In the process of building programs (through processes of mutation, crossover and reproduction), GP shows predictions which are slightly over predicted as compared to ANN (Refer Fig. 3) and thus GP shows a performance less as compared to ANN. Addition of material properties as Soft coefficient of sand and maximum size of aggregates as input parameters in developing ANN and GP models helps in predicting concrete strength is slightly better than the models with input parameters as mix design proportions. Though GP2 shows a reduction in R value as compared to GP1, the reduction is not very significant. Thus it can be said that inclusion of material properties as input parameters in development of models is beneficial for to capture the underlying phenomenon of the subject in detail. Figs. 2 and 3 show the scatter plot for ANN1 and GP2 respectively. The scatter plots for ANN1, ANN2 and GP2 do not exhibit an obvious under or over prediction. The trend of predicting concrete strength by GP1 is as shown in Fig. 4. It also shows ANN predicted values to be in tune with the Observed values but slight over prediction of strength in GP.

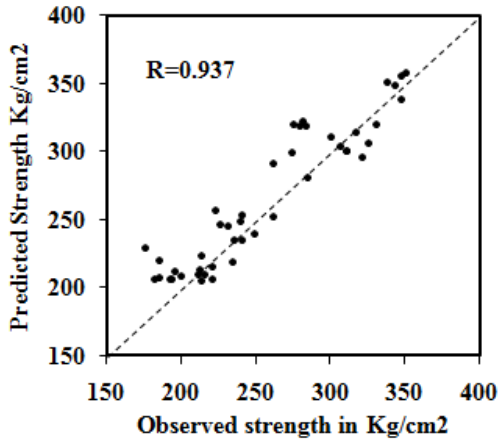

Fig. 2. Scatter plot for ANN1.

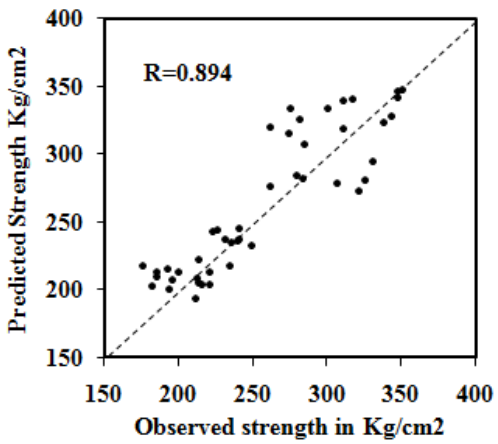

Fig. 3. Scatter plot for GP2.

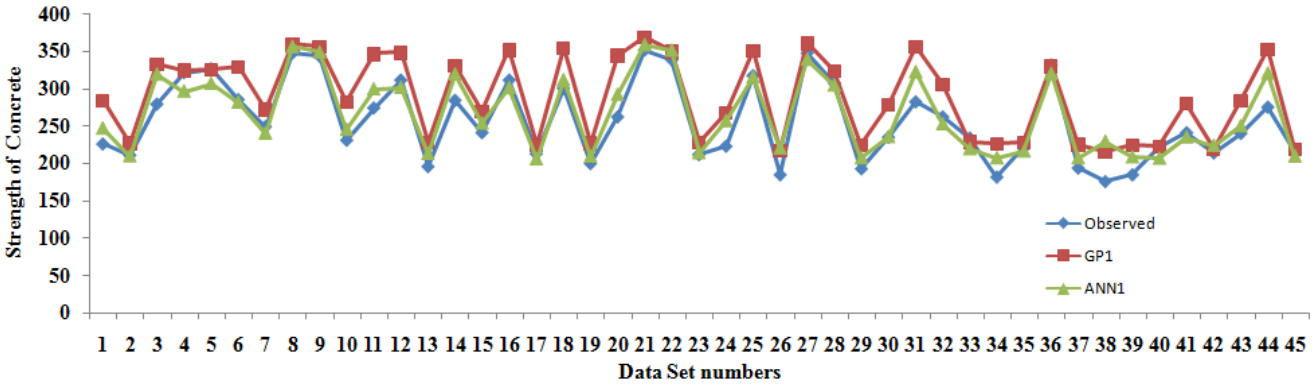

Fig. 4. Comparison between actual and predicted values for GP1.

5.1. Knowledge extraction

Knowledge extraction as mentioned in the previous section is done to understand the influence of input parameter/s on the output. By using the procedure developed for extraction (Londhe and Shah, 2016), the histograms for model ANN1 and ANN2 were drawn and are shown in Figs. 5 and 6.

Fig. 5 show higher influence of C followed by SA, G2 and G1 content. A similar influence can also be seen in ANN2. Thus it can be said that inclusion of mix design parameters in respective proportions is important and its influence as per the domain knowledge is being calculated by ANN through judicious allocation of weights and biases. Strength of concrete is inversely proportional to water/cement ratio in hardened state (Shetty, 2005).

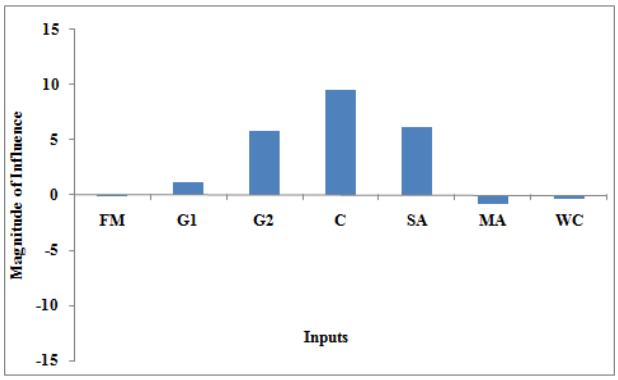

Fig. 5. Influence of inputs for ANN1.

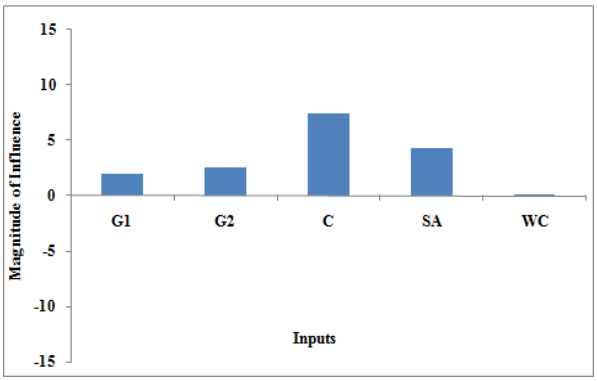

Fig. 6. Influence of inputs for ANN2.

For given cement content when the water cement ratio increases a decrease in the strength can be seen. This can be seen through negative influence of WC in ANN2. ANN1 however shows a direct influence of water to cement ratio on concrete strength; however the influence seen is of very small magnitude (01.3) as compared to other parameters. The magnitude of influence for Soft coefficient of sand (FM) and Maximum size of aggregate (MA) is also been shown by Fig. 6. Increase in soft coefficient of sand implies increase in coarseness of sand

which shows a decrease in strength for a constant water cement ratio (Shetty, 2005). Also, lower strength of concrete is attributed towards the larger MA which gives lower surface area for developments of gel bonds. More heterogeneity in the concrete is seen when bigger aggregate size is used, which prevents the uniform distribution of load when stressed. Also internal bleeding can be seen and weaker the transition zone due to the development of micro cracks. This leads to lower compressive strength in concrete (Shetty, 2005; Neville, 2012). Thus it can be said that concrete strength is inversely proportional to the maximum size of aggregate, which can be seen from magnitude of influence for the said parameter. Knowledge extraction done by the said method thus can serve as a guideline towards input selection in development of ANN models. Genetic Programming on other hand evolves an equation or formula relating to the input and output variables. A major advantage of GP approach is its automatic ability to select input variables that contribute beneficially to the model and disregard those that do not. GP can thus reduce substantially the dimensionality of the input variables (Bishnoi, 2014). The equations developed in GP1 and GP2 shows the presence of all input parameters which are influential in predicting strength of concrete, which is also in tune with the fundamental knowledge of concrete technology. The inverse proportionality of WC with strength of concrete is shown in Eqs. (8) and (9).

6. Conclusions

Concrete being a complex material, modelling its behaviour is a difficult task. In the current work an attempt is made to predict strength of concrete using ANN and GP. Comparative analysis of ANN and GP techniques show that ANN predicts 28 day strength of concrete with good accuracy as compared to GP which can be evident from the higher R values. The performance statistics validated by lower NRMSE, E and RMSE values also show a good performance of ANN as compared to GP in all the models. Prediction of concrete strength can be done satisfactorily with the presence of mix design parameters i.e. mix proportions as input parameter and presence of material properties as FM and MA show slight increase the performance of models.

ANN shows the output in the form of weights and biases in which the knowledge about the problem is locked. Thus, analyzing the weights and biases in ANN and extracting the knowledge locked up in them done was done using the knowledge extraction model. This show that ANN1 and ANN2 show the influencing parameters as C and SA followed by G1 and G2 which is in tune with the basic domain knowledge. Thus ANN can't be just labelled as a black box and can be said as a Grey box. Genetic programming on the other hand displays the influence of input parameters through the presence of relevant parameters in the equation. Influence of WC ratio is shown as inverse in ANN1 which is as per the domain knowledge of concrete technology.

ANN thus predicts strength of concrete better than GP and can display the output in terms of weights and biases for a given set of input. ANN however has a limitation of not been able to provide standalone equations which can be done in GP. GP on the other hand is a powerful tool and can open a new field for efficient explicit equations of many civil engineering problems.

Appendix A. Knowledge extraction from ANN

A.1. Input to hidden layer

Fig. 7 shows the diagrammatic representation of a typical three layered feed forward network with 3 input neurons, 2 hidden neurons and 1 output neuron.

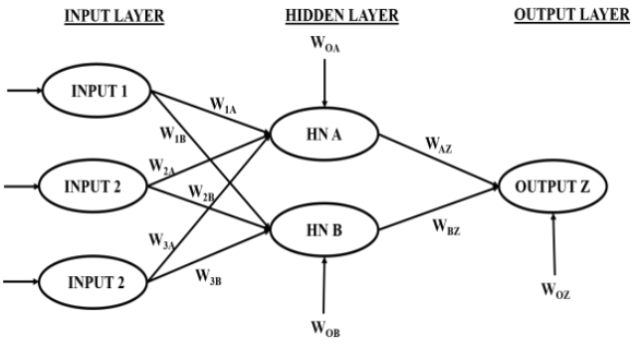

Fig. 7. Basic ANN architecture.

It can be seen from Fig. 7 that each hidden neuron in the hidden layer receives weights from all the inputs in the network. Thus, each hidden neuron contains a fraction of weight from each input. The fraction of a particular input can be calculated by taking a ratio of the weight of that particular input with the total weight from all inputs. For example, from Fig. 7, the fraction of first input in the first hidden neuron can be given by Eq. (4). Similarly, the fraction of each input on each of the hidden neurons can be calculated.

$$F_{1A} = W_{1A}/(W_{1A} + W_{2A} + W_{3A}). \quad (4)$$

When the network is trained, a bias (W_{OA} and W_{OB}) is added to each hidden neuron. This bias can be divided into parts as per the fraction of weight of each input to that hidden neuron, thus assigning a part of bias to each of the input, through each of the hidden neurons. The bias assigned to the first input through the first hidden neuron can be calculated by Eq. (5).

$$W_{OA1} = W_{OA} \, X \, F_{1A}. \quad (5)$$

The total contribution of a particular input, on the hidden layer, can then be determined by addition of the fractions of its influence and fraction of the bias through all the hidden neurons. The total influence of input 1 can be calculated as given in Eq. (6).

$$C_1 = (F_{1A} + W_{OA1}) + (F_{1B} + W_{OB1}). \quad (6)$$

A.2. Hidden to output layer

Each hidden neuron of the hidden layer is connected to the output with the layer weights. The layer weight from one hidden neuron to the output again, consists of fractions of each of the inputs that were calculated earlier. Thus, the layer weight from a hidden neuron to the output is again divided into parts as per the fractions of the influence of inputs in that particular hidden neuron. The contribution of the first input on the output through the first hidden neuron can be calculated by Eq. (7). Similarly, the contribution of the first input through all the hidden neurons can be calculated and their sum would give the total influence of that input on the output through the layer weights, as seen in Eq. (8). The total influence again would be a sum of these influences and the bias that is added to the output layer (W_{OZ}).

$$L_{1AZ} = W_{AZ} \, X \, F_{1A} , \tag{7}$$

$$L_1 = L_{1AZ} + L_{1BZ} + W_{OZ} . \tag{8}$$

Thus, the total influence of the first input on the output can be given by Eq. (9).

$$I_1 = C_1 + L_1 . \tag{9}$$

The procedure is repeated for each of the inputs, and the results are plotted as histogram.

Appendix B. Weights and biases for ANN2

Input layer to hidden layer Weights

0.1436	1.2858	5.267	7.6692	5.2026	-0.2094	0.2353
0.135	1.2472	5.2313	7.6697	5.1958	-0.2515	0.1693
0.1321	1.2315	5.217	7.67	5.1932	-0.2685	0.1428
0.1483	1.3058	5.2858	7.6687	5.2061	-0.1877	0.2696
0.142	1.2808	5.2623	7.669	5.2016	-0.2151	0.2263
0.1381	1.2632	5.2459	7.6694	5.1985	-0.2343	0.1961
0.1457	1.2956	5.2761	7.6688	5.2042	-0.199	0.2518
-0.1056	0.8213	4.6288	7.893	5.1426	-0.852	-0.4293
-0.136	0.8283	4.7946	7.7097	5.2305	-0.7434	-0.2797
-0.0251	0.8459	4.2365	8.2921	4.9021	-1.1892	-0.8141
-0.0633	0.8266	4.3872	8.1406	5.0034	-1.047	-0.6592
-0.0394	0.8376	4.2867	8.2415	4.9376	-1.14	-0.7614
0.1108	0.9812	5.013	7.6632	5.1757	-0.5143	-0.2189
0.1164	0.943	4.986	7.6614	5.1709	-0.553	-0.2749
0.1107	0.9786	5.0112	7.6627	5.1756	-0.5169	-0.2224

Bias

0.017
0.0574
0.073
-0.004
0.0229
0.0414
0.0072
0.7573
0.6489
1.2133
1.0104
1.1419
0.2808
0.3009
0.2829

Hidden layer to output Weights

0.2612
0.1753
0.1408
0.3046
0.2489
0.2099
0.2817
-0.1404
-0.4352
0.6226
0.3137
0.5168
-0.3147
-0.4033
-0.3198

Bias

-0.7919

REFERENCES

Ahmet OZ, Murat PB, Erdogan O, Erdog K, Naci C, Bhatti A (2006). Predicting the compressive strength and slump of high strength concrete using neural network. *Construction and Building Materials*, 20, 769–775.

Behfarnia K, Khademi F (2017). A comprehensive study on the concrete compressive strength estimation using artificial neural network and adaptive neuro-fuzzy inference system. *Iran University of Science & Technology,* 7(1), 71-80.

Bowden GJ, Dandy GC, Maier HR (2005). Input determination for neural network models in water resources applications. Part 1—background and methodology. Journal of Hydrology, 301(1-4), 75–92.

Bishnoi U (2014). Mathematical modeling for bond strength for Recycled coarse aggregate concrete using Genetic Programming. *M.E Thesis*, Thapar University.

Bhattacharya B, Solomatine P (2005). Neural networks and M5 model trees in modeling water-level- discharge relationship. *Neurocomputing*, 63, 381-396.

Deshpande NK, Londhe SN, Kulkarni SS (2014). Modeling compressive strength of recycled aggregate concrete by Artificial Neural Network, Model Tree and Non-linear Regression. *International Journal of Sustainable Built Environment,* 3, 187–198.

Dias WPS, Pooliyadda SP (2001). Neural networks for predicting properties of concretes with admixtures. *Construction and Building Materials.* 15, 371-379.

Gorphade VG, Sudarsana HR, Beulah M (2014). Development of Genetic Algorithm based Neural Network Model for Predicting Workability and Strength of High Performance Concrete. *International Journal of Inventive Engineering and Sciences*, 2(6), 1-8.

Gandomia AH, Mohammadzadeh D, Pérez-Ordó˜nezc JL, Alavi AH (2014). Linear genetic programming for shear strength prediction of reinforced concrete beams without stirrups. *Applied Soft Computing*, 19, 112–120.

Khademi F, Jamal SM, Deshpande N, Londhe S (2016). Predicting strength of recycled aggregate concrete using artificial neural network, adaptive neuro-fuzzy inference system and multiple linear regression. *International Journal of Sustainable Built Environment,* 5(2), 355-369.

Khademi F, Akbari M, Nikoo M (2017). Displacement determination of concrete reinforcement building using data-driven models. *International Journal of Sustainable Built Environment*, 6(2), 400-411.

Kahramanli K, Allahverdi N (2001). Rule extraction from trained adaptive neural networks using artificial immune systems. *Expert Systems with Applications*, 36(2), Part 1, 1513–1522.

Koza J (1992). *Genetic Programming: On the Programming of Computers by Means of Natural Selection*. A Bradford Book. MIT Press, 1992.

Kumar P, Kumar A (2015). Prediction of compressive strength using genetic programming involving NDT results. *BTech thesis*, National Institute of Technology, Rourkela, 2015.

Londhe SN, Shah S (2016). Knowledge extraction from artificial neural network models developed for evaporation. *20th IAHR-APD*, August 28-31, Colombo, 2016.

Londhe SN, Dixit PR (2012). Genetic Programming: A Novel Computing Approach in Modeling Water Flows Genetic Programming – New Approaches and Successful Applications. Chapter 9. Licensee InTech. 2012.

Londhe SN (2009). *Towards predicting water levels using artificial neural network.* IEEE Xplore Oceans 2009, 11-14 May 2009, Europe, 1-6.

Lee KM, Lee HK, Lee SH, Kim GY (2006). Autogenous shrinkage of concrete containing granulated blast-furnace slag. *Cement and Concrete Research,* 36(7), 1279–1285.

Legates DR, McCabe GJ (1999). Evaluating the use of "goodness of fit" measures in hydrological and hydro climatic model validation. *Water Resources Research,* 35(1), 233-24.

Mukherjee A, Sudip NB (1997). Artificial neural networks in prediction of mechanical behavior of concrete at high temperature. *Nuclear Engineering and Design,* 178(1), 1-11.

Meltem O, Birgül K, Turan O (2008). Comparison of concrete strength prediction techniques with artificial neural network approach. *Building Research journal,* 56, 23-36.

Ni HG, Wang JZ (2000). Prediction of compressive strength of concrete by neural networks. *Cement and Concrete Research,* 30, 1245-1250.

Neville AM (2012). Properties of Concrete. Pearson Education, USA and UK.

Oner A, Akyuz S (2007). An experimental study on optimum usage of GGBS for the compressive strength of concrete. *Cement and Concrete Composites.* 29(6), 505–514.

Phukoetphim P, Shamseldin AY, Melville BV (2014). Knowledge Extraction from Artificial Neural Networks for Rainfall-Runoff Model Combination Systems. *Journal of Hydrologic Engineering*, 19(7), 1422-1429.

Shetty MS (2005). Concrete Technology, 17th edition. S. Chand and Company, New Delhi.

Sarıdemir M (2010). Genetic programming approach for prediction of compressive strength of concretes containing rice husk ash. *Construction and Building Materials*, 24, 1911–1919.

Challenge Journal of Concrete Research Letters

Research Article

Acoustic emission signal 'peak amplitude-distribution' analysis related to concrete fracture under uniaxial compression

R. Vidya Sagar *

Department of Civil Engineering, Indian Institute of Sicence, Bangalore 560 012, India

ABSTRACT

Acoustic emissions (AE) released during the compressive fracture of cementitious materials have been subjected to analysis using 'AE based *b*-value' to study the fracture process. Identification of the 'AE sources locations' in three dimension is not always possible. With a minimum number of AE sensors mounted on the test specimen and by using the AE based *b*-value analysis, it is possible to study fracture process and the damage status in solids. The *b*-value of AE is calculated using the Gutenberg–Richter empirical relationship (G-R law), which is available in seismology. The details related to original G-R relation and it's suitability for AE testing were discussed. In this article it has been tried to look into the variations of the AE based *b*-value in cementitious test specimens prepared with different cementitious mixture proportions. Effect of (i) coarse aggregate size in cementitious materials (ii) loading rate during compressive fracture process (iii) age of concrete on *b*-value variation were discussed. The trend of variation in AE based *b*-value during fracture process in concrete and mortar was different. It was observed that when the compression toughness of the cementitious material increases, higher *b*-values were observed. When the loading rate was high, quick cracking occurred and lower *b*-values were observed. As the coarse aggregate size in the cementitious material increases, the cumulative AE energy was higher. The reason may be due to the compression toughness of the cementitious material. The AE based *b*-value is useful to identify the different stages of compressive fracture process in solids.

ARTICLE INFO

Article history:
Received 3 August 2018
Revised 19 September 2018
Accepted 25 September 2018

Keywords:
Non-destructive testing
Concrete
Fracture
Acoustic emission
Uniaxial compression

1. Introduction

Monitoring of crack development in concrete structures *in-situ* is required and also compulsory in case of some structures. For example, in case of pressure vessels, nuclear power plant structures, monitoring of crack initiation, coalescence, propagation more or less required continuously. Because, the potential loss in concrete strength, cracking that might occur with time. Therefore, structural health monitoring (SHM) of concrete structures is necessary. Ageing of concrete structures (residential buildings, public buildings), heavy loads on bridges (due to increasing traffic volume), aggressive environment (acid rains, air-pollution, and salts) are few causes behind the necessity for the frequent health monitoring of concrete structures. It would, therefore, useful to have available non-destructive testing (NDT) methods for monitoring concrete structures that is sensitive enough to indicate sufficient warning of an impending collapse of structures. Also to know whether cracks are developed or not in concrete structures under service loads NDT method are useful (Nair and Cai, 2010; Kalayanasundaram et al., 2007; Holford, 2000). Based on non-destructive testing observations repairs could be made before the damage becomes rigorous.

* *Corresponding author*. Tel.: +91-80-2293-3210 ; Fax: +91-80-2360-0404 ; E-mail address: rvsagar@iisc.ac.in (R. Vidya Sagar)
ISSN: 2548-0928 / DOI: https://doi.org/10.20528/cjcrl.2018.03.003

1.1. Brief introduction to acoustic emission testing

Acoustic emission (AE) testing is a NDT method to monitor fracture process in real time and also to assess the damage status in solids/structures. By using this passive NDT method the active cracks and their characteristics can be studied. The entire concrete structure can be monitored for cracks in a single inspection. The real time progress of fracture process can be studied by mounting minimum required number of AE sensors on the structure (Gross and Ohtsu, 2008; Ohtsu, 1998). During fracture process in solids the strain energy is released in the form of elastic waves (or stress waves) and reach to the surface of the solid/structure. AE refers to the generation of transient elastic waves during the rapid released of energy from localized sources within a solid (Kalyanasundaram et al., 2007). By mounting the required number of PZT sensors on the test specimen or structure these elastic waves can be recorded. Subsequently, the PZT sensors convert the elastic waves into electrical signals. A schematic representation of a typical AE signal and corresponding parameters are shown in Fig. 1. By using these signals the fracture process occurred in real time can be studied in solids (RILEM TC-ACD, 2012a; 2012b, 2012c).

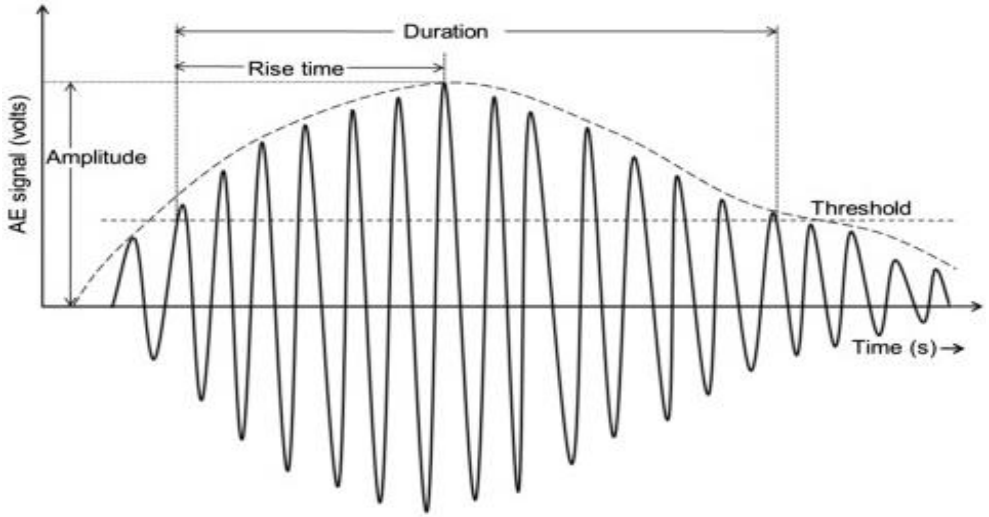

Fig. 1. Schematic representation of an AE signal and corresponding parameters (Datt et al., 2015).

1.2. AE based b-value

Researchers confirmed that there is a close analogy exists between AE produced during fracture process in solids and the seismic waves caused due to earthquake (Rao and Lakshmi, 2005). Analogous to the occurrence of earthquakes, during fracture process in solids, higher amplitude acoustic emissions (stress waves caused by internal material fracture or micro seismic activity) released less in number and lower amplitude AE more in number as shown in Fig. 2. It can be observed that AE peak amplitudes greater than 60 dB are less when compared with lower amplitude AE hits.

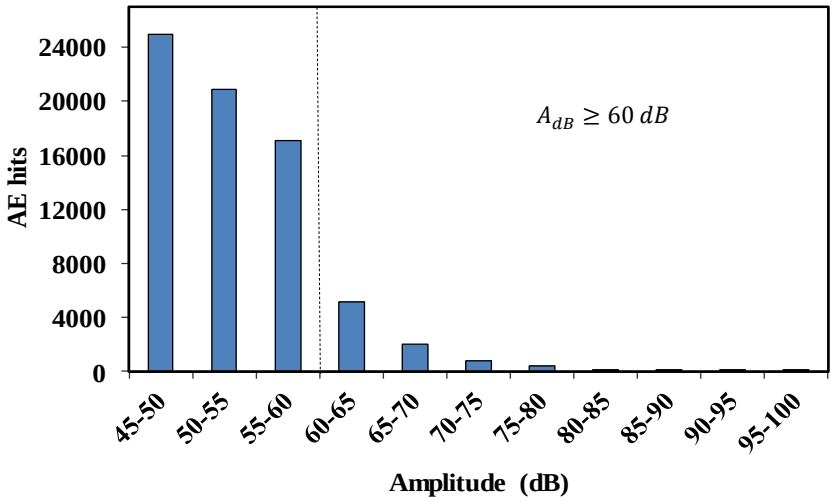

Fig. 2. Distribution of the number of AE hits versus AE peak amplitude.

Also, AE released during fracture process in solids are similar to the P-waves that generated during occurrence of earthquake. Because of similarities between occurrence of earthquakes and happening of AE events during fracture process in solids, researchers attempted to use Gutenberg-Richter law available in seismology (Gutenberg and Richter, 1954; Mogi, 1964). However, researchers modified the Gutenberg-Richter law to study frequency of occurrence-amplitude distribution of AE released during fracture process in solids (Colombo et al., 2003).

$$\mathbf{log_{10}N(A) = a - b\left[\frac{A_{dB}}{20}\right]}. \quad (1)$$

In Eq. (1), A_{dB} is the peak amplitude of the AE (hits or events) in decibels. b is the AE based *b*-value. *N(A)* is the number of AE hits of amplitude greater than A. 'a' is constant. The details about Eq. (1) and the theory of "AE based *b*-value" are discussed in Appendix-A.

2. Literature Review

The AE based *b*-value is a parameter to study damage status and fracture process in solids (Colombo et al., 2003). This *b*-value has been used for structure damage evaluation by several researchers. Colombo et al. (2003) studied the variation in the AE based *b*-values for a reinforced concrete (RC) beam subjected to incremental cyclic loading. The variation in *b*-values was compared to the micro-cracking and macro-cracking observed during the fracture process. It was concluded that, minimum *b*-value indicates the formation of macro-cracks and maximum *b*-value denotes micro-cracking. The AE based *b*-value analysis has been used for structural damage evaluation by several researchers Shiotani et al. (2001), Kurz et al. (2006), Ko and Yu (2009) Schumacher et al. (2011). Proverbio et al. (2011) assessed damage in post-tension concrete viaduct using *b*-value analysis and concluded that a decrease in b-value could be an indication of an impending fracture. Schumacher et al. estimated the operating loading on RC highway bridges with *b*-value analysis. Carpinteri et al. (2006) observed that the AE based *b*-value ranges from 1.5 to 1.0 when the fracture process progress in the critical state to final collapse. Vidya Sagar and Rao (2014) investigated the effect of loading rate on *b*-values related to fracture process in reinforced concrete (RC) flanged beams.

Though, AE based *b*-value was accepted to be a suitable parameter to characterize various stages of fracture process in solids, the studies related to the influence of (i) concrete strength (ii) coarse aggregate size in concrete (iii) rate of loading (iv) curing period of concrete on *b*-value when concrete is under uniaxial compression are minimum. Lack of complete understanding of AE based *b*-value, when there is a change in cementitious material mixture proportion, insufficient statistics of experimental data still keeps the AE based *b*-value analysis problem opened for further discussion. The further work done in this study is that the AE based *b*-value is used to study fracture process in cementitious materials under uniaxial compression and discussed this useful damage assessment parameter in detail.

3. Research Significance

Characterizing different stages of fracture process in concrete structures using AE testing provide an early warning for any probable damage in concrete structures (Grosse and Ohtsu, 2008; Uchida et al., 2011). It is known that concrete structures are no longer maintenance free. For *in-situ* monitoring of damage in concrete structures, the variation in *b*-values provides useful information related to micro-cracking and macro-cracking. Since it is not easy to obtain 3-D source location data of high frequency and low amplitude AE. With a minimum required number of AE sensors the fracture process in a concrete structures can be studied using AE based *b*- value. Concrete structures have many structural components associated with it and the column is one of the most important compression members as it supports the whole structure. In some cases short-columns are required for construction. Uniaxial compression has been important in studying behavior of short columns. The results of the present study lead to understanding of the fracture process in concrete subjected to uniaxial compression and also may be further application of AE testing in structural health monitoring of concrete structures.

4. Experimental Procedure

Unconfined uniaxial compression tests were conducted and monitored the deformation and failure behavior of a set of cement concrete and mortar cylindrical specimens (150 mm diameter and 300 mm height) in Structures Laboratory, Department of Civil Engineering, Indian Institute of Science Bangalore, India. The tests were carried out under displacement control at a constant rate of 0.005 mm/s and 0.002 mm/s using a servo-controlled testing machine (1200 kN capacity, MTS machine) and by recording the released AE simultaneously. The rate of loading is assumed (not as per any standard) to test the samples in the laboratory. This kind of MTS machine is controlled by an electronic closed-loop servo-hydraulic system. It is therefore possible to perform tests under load or displacement control.

4.1. Materials

Three different cementitious materials namely, Concrete-I, Concrete-II and cement mortar were considered in this study. Concrete-I consists maximum coarse aggregate size of 20 mm and its mixture proportion per 1 cubic meter (by mass) was 414:729:1143 (cement: fine aggregates: coarse aggregates). The water/cement (w/c) ratio was 0.46. Concrete-II mixture proportion was 450:716:1100 and its w/c ratio was 0.526. For cement mortar specimens 1343 kg/m^3 sand, 285.5 liters water and 543 kg/m^3 cement were used. The difference between Concrete-I and Concrete-II is not the maximum grain size of the aggregate alone. water/cement ratio, cement dosage are also different. However, the aim is to study the influence of the coarse aggregate on AE peak amplitude distribution.

4.2. Test specimens

Eleven specimens were cast using each cementitious materials namely, Concrete-I, Concrete-II and Cement mortar (total 31 specimens). Cement mortar specimens were tested to study the coarse aggregate influence on AE characteristics of cement concrete. All specimens were cast in mild steel cylindrical molds with a diameter of 150 mm and height of 300 mm. One end of the steel mold was capped to form a cylinder. Concrete was placed in nearly 100 mm thick layer and immediately compacted. An internal needle vibrator was used to ensure proper compaction of the cementitious mixtures. Test specimens were kept in the molds for the first 24 hours, with the top surface covered with a wet gunny bag. At the age of 24 hours the specimens were removed from their molds. Specimens were placed in a water tub until the time of testing. Before testing, the specimens were taken out from water tub and kept for drying. The specimens were tested for different curing periods of 7 days, 15 days and 28 days for Concrete-I, 9 days, 17 days and 28 days for Concrete-II and 7 days, 15 days and 28 days for cement mortar. The uniaxial compressive strength of test samples (cylinders) at various curing period for Concrete-I, Concrete-II and Cement mortar is shown in Fig. 3.

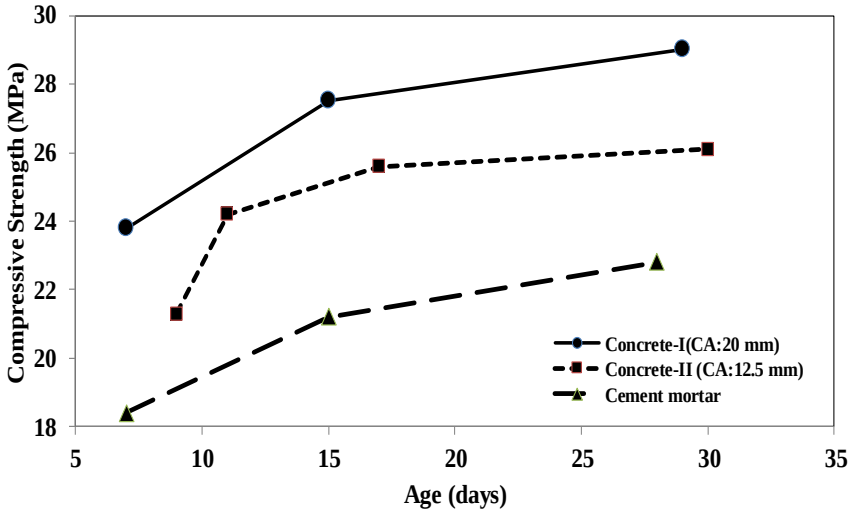

Fig. 3. Compressive strength (cylinder) variation in the three cementitious materials with age.

4.3. AE recording system

The AE signal parameters were recorded via the AE monitoring system during the uniaxial compression of the cementitious materials because the time history of the AE characteristic parameters reflect how fracture process occur and evolve. For AE signal detection, two resonant type differential AE sensors (57 kHz) with preamplifier gain of 40 dB were used. The use of two AE sensors is usual for monitoring the AE parameters in laboratory. In this study, recording of AE event locations is not attempted. The AE monitoring system was manufactured by Physical Acoustic Corporation (PAC) NJ, USA. AE^{WIN} SAMOS software and R6D resonant sensors were used. Each AE sensor was attached to the surface of the specimen at a height of 150 mm from bottom of cylinder on either sides of the specimen. The sensor surface was 17.5 mm in diameter and 16.25 mm in height. The surface of the test specimen was thoroughly cleaned and vacuum silicon grease was used as a couplant to both sensor surface and area of sensor location on the test specimen. Brown color gum tape was used to attach the sensor to test specimen and also to apply pressure on sensor to maintain their contact with specimen's surface. A threshold of 40 dB was set to screen out surrounding noise and the AE activity generated due to friction between the top and bottom surface of the specimen with end plates. AE monitoring system parameters, namely, PDT is 200 µs, HDT is 400 µs, HLT is 500 µs and for maximum duration 1000 µs were set. The AE data acquisition system was setup to acquire AE signal parameters namely, hits, peak amplitude, counts, energy, duration, signal strength, absolute energy, time, average frequency. The experimental setup is shown in Fig. 4(a). In this study, two AE sensors were mounted on the test specimen as shown schematically in Fig. 4(b).

Fig. 4(c) indicates the optimal frequency response of used AE sensor. It can be observed that at 54.7 kHZ frequency the sensors had highest sensitivity at 77.1 dB amplitude. In other words, sensitivity stands for least measurable physical parameter. The AE sensor has a sensitivity and frequency response over the range of 35 kHz - 100 kHz. The peak load, rate of loading, age of concrete and AE parameters namely, counts and energy recorded for all test specimens were shown in Table 1.

5. Procedure to Compute AE based *b*-value

5.1. AE amplitude distributions related to concrete under uniaxial compression

Fig. 5 shows cumulative number of AE hits on the Y-axis (log scale) and amplitude of AE in dB on the X-axis. All the

AE signals were found to fall in the amplitude range of 40 dB to 100 dB. A large number of AE hits had smaller amplitudes and the distribution shows a descending gradient. The slope of the 'linear descending branch' of the cumulative distribution graph is known as the "AE based *b*-value". There is a marked change in the trend of the amplitude distribution after the onset of micro cracking in the Concrete-I test samples at ~20% failure stress (σ_f) as shown in Fig. 5.

Table 1. Test specimen details, rate of loading and recorded peak load and AE parameters.

Cementitious material	Age (days)	Specimen	Peak load (kN)	Rate of loading (micron/s)	Total AE counts	Total AE energy (Volt-s)	Time duration of the test (s)
Concrete-I	7	C1_7A	401.1	5			730
		C1_7B	438.9	5	542457	3301627	354
		C1_7C	424.2	5	874633	6630822	804
	15	C1_15A	435.3	5	383468	2708549	860
		C1_15B	587.1	5	355480	1870588	708
		C1_15C	439.1	5	416198	4379934	804
	29	C1_29A	456.3	5	502290	4877430	460
		C1_29B	523.1	5	479272	4612799	780
		C1_29C	337.3	5	985818	8059748	1265
		C1_29D	640.9	5	360657	3359106	540
		C1_29E	606.3	5	257030	3221477	470
Concrete-II	9	C2_9A	378.1	5	327670	870482	863
		C2_9B	378.6	5	694363	2464721	1112
		C2_9C	377.5	5	583085	2934222	954
	11	C2_11A	385.4	5	599407	3794971	830
		C2_11B	471.6	5	348349	3195094	710
	17	C2_17A	407.1	5	90567	2254411	860
		C2_17B	498.7	5	114719	3294762	840
	30	C2_30A	461.9	2	225574	2385511	2238
		C2_30B	452.6	5	89919	1654119	876
Cement Mortar	7	M_7A	336.8	5	216273	854441	624
		M_7B	299.0	5	300999	1178567	714
		M_7C	341.3	5	276197	1074503	642
	15	M_15A	408.8	5	395938	2495569	774
		M_15B	346.75	5	360429	2307427	684
		M_15C	367.4	5	378386	2433103	684
	28	M_28A	438.6	2	465076	1932337	1788
		M_28B	346.2	2	398123	1192909	2550
		M_28C	349.9	5	304666	1283757	805
		M_28D	406.7	5	348197	1011627	730
		M_28E	459.6	5	262887	1370554	790

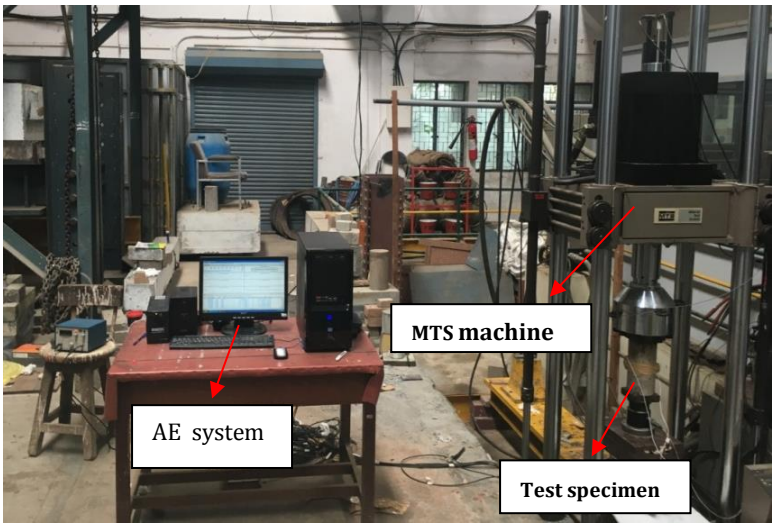

Fig. 4(a). Experimental setup in Structures Laboratory, Department of Civil Engineering, Indian Institute of Science Bangalore, India.

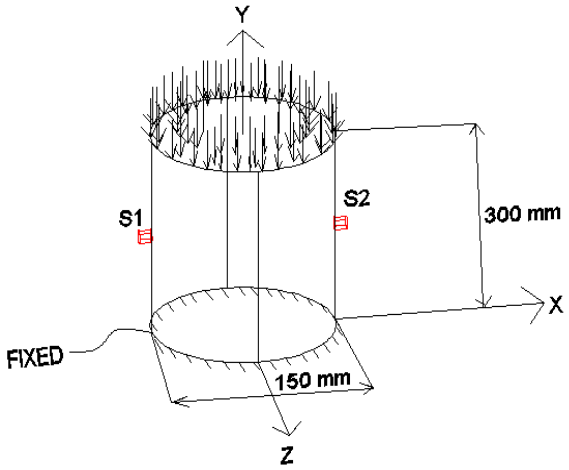

Fig. 4(b). Schematic diagram of the test specimen in isometric view (S1&S2 indicates AE sensors).

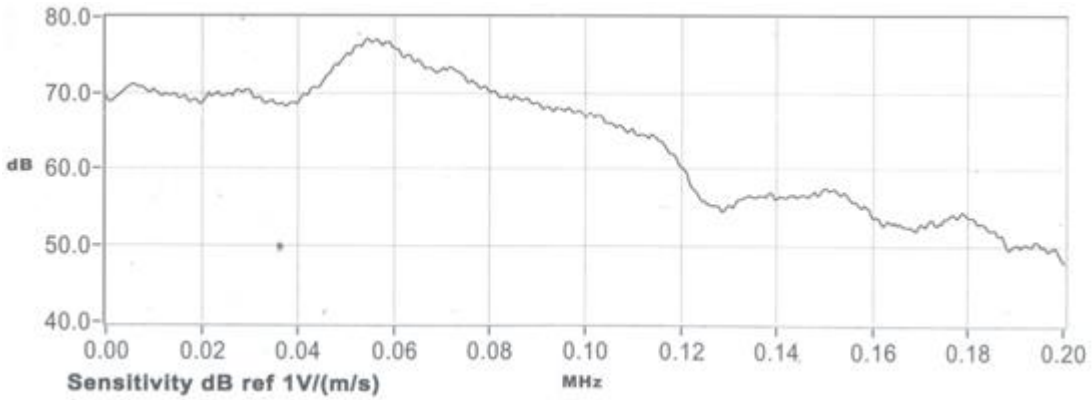

Fig. 4(c). Frequency response of the used AE sensor as given by the manufacturer of AE system. Resonant type AE sensor's frequency characteristics, maximum amplitude 77.1 dB recorded at peak frequency 54.7 kHz (PAC, AE WIN SAMOS user manual, 2005).

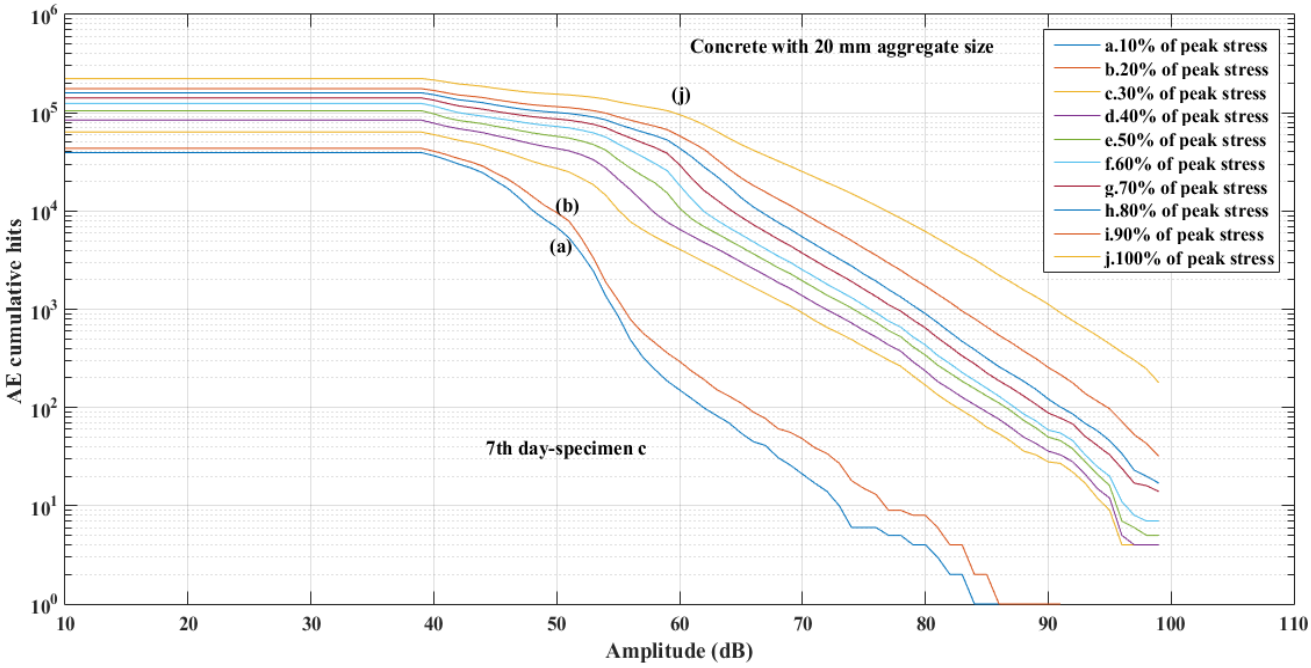

Fig. 5. AE cumulative frequency of occurrence–amplitude distribution graphs corresponding to different stress ranges. The graphs were obtained from the AE recorded during deformation and progressive failure of Concrete–I test specimen under uniaxial compression (Rao and Lakshmi, 2005).

The change of slope of the line plotted between AE cumulative hits and amplitude (also known as *b*-value) indicates the occurrence of fracture process in the solid. From Fig. 5, it can be observed that as the external force applied on the test specimen increases the slope of the line changes as observed in lines (a)-(j) in Fig. 5.

5.2. AE magnitude variation with external stress

Plot between AE frequencies of occurrence-amplitude distributions does not show a single straight line, and different ranges of amplitude indicated different lines. This can be observed in Fig. 6, where a three sets of 'cumulative AE magnitude distribution' graphs are shown after applying the necessary correction to convert AE amplitude to magnitude. In the initial stages of compressive fracture process when the stress range is low (0–20% of σ_f) the AE population is less, the cumulative AE hit-magnitude distribution plot is almost linear. Whereas in the higher stress ranges, the cumulative AE hit magnitude distribution graph shows a 'fairly good linear relationship' in the magnitude range from 2.90 to 4.40, although the polynomial fit yields better correlation (Fig. 6). AE frequency of occurrence-magnitude distribution is linear during early stages of loading and appears polynomial curve at stresses near failure as shown in Fig. 6. However, the distribution graph shows a 'fairly good linear relationship' in the magnitude range from 2.7 to 4.4.

By following Colombo et al. (2003), the AE based *b*-value was computed. Using Fig. 7 number of hits for group was determined. The cumulative frequency of occurrence - amplitude distribution graphs have been obtained using a Matlab program.

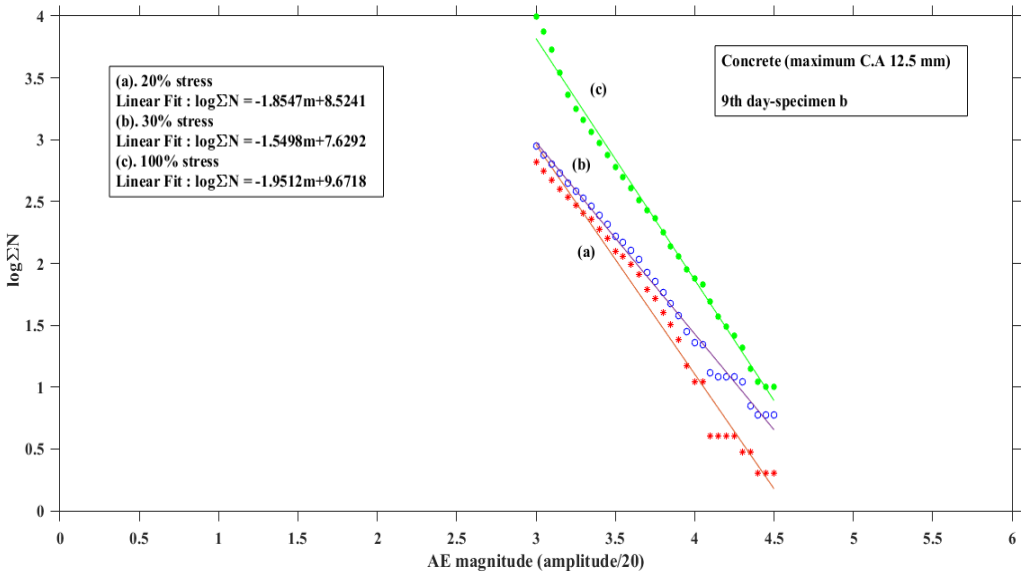

Fig. 6. Cumulative frequency of occurrence-magnitude distribution plots of AE corresponding to three stress ranges (Rao and Laskhmi, 2005).

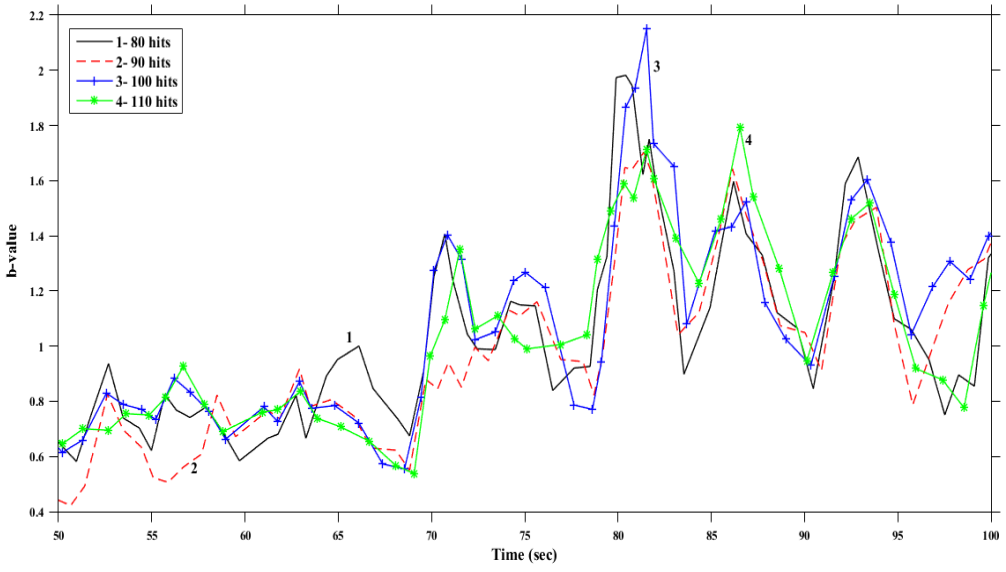

Fig. 7. AE based *b*-value variation with time. *b*-value was calculated using (i) group of 80 hits, (ii) group of 90 hits (iii) group of 100 hits, and (iv) group of 110 hits (Colombo et al, 2003).

6. Results and Discussion

6.1. AE based b-value variation related to cement concrete under uniaxial compression

The variation of *b*-values versus load and time is shown in Fig. 8. It is observed that a sharp changes in *b*-value corresponding to the various stages such as formation and growth of stable cracks, crack coalescence and unstable cracks during fracture process. During the early stages of loading (stage-I), AE released due to the closure and rubbing of pre-existing micro-cracks in the concrete began to show a high *b*-value. A sudden dip in *b*-value indicates the dominance of AE events of larger amplitude at that time.

Micro cracks are present in a concrete specimen. These cracks may be present due to differential temperatures from hydration, differential drying, and excessive bleeding of water near aggregates. Even before the application of load on the specimen micro cracks are present in the interfacial transition zone (ITZ) between mortar matrix and coarse aggregate (Neville, 2011; vanMier 1997). Cracks in ITZ are formed at boundary of coarse aggregate and mortar matrix due to flow of soft matrix around coarse aggregate. Lateral deformation in matrix is much higher than that in aggregate. This unevenness causes development of shear stresses on top and below of coarse aggregates. In stiff aggregates these stresses lead to formation of shear cones, whose occurrence has been confirmed by many researchers. In case of light weight aggregates instead of going around the aggregates cracks go through them, so tensile splitting prevails (vanMier, 1998).

According Mehta (2006), in the Ist stage, from start of the test to till 30% of peak stress (σ_f) interfacial cracks remain stable. However, until about 50% of σ_f, a stable system of micro cracks appears to exist in the ITZ. This is Stage -II and at this stage the matrix cracking is negligible. At 50% to 60% of σ_f, cracks begin to form in the cement matrix. With further increase in uniaxial stress to 75% of σ_f, not only does the crack in the ITZ becomes unstable but also the creation and propagation of cracks in the cement matrix increases, causing the stress-strain curve to bend considerably toward the horizontal. This is Stage-III.

At 75% to 80% of σ_f, the rate of 'strain energy release' seems to reach the critical level necessary for crack growth under sustained stress, and the concrete material strains to failure. In short, above 75 % of σ_f, with increasing stress very high strains are developed. This indicates that the crack is becoming continuous due to the rapid propagation of cracks in both the cement matrix and the ITZ. This is the final stage (Stage-IV).

In near peak region the cracks are large and remain stable only when certain conditions are met. At around 80-90% of σ_f, there comes a point where the volume of the specimen becomes minimum. It is because till this point crack opening in lateral direction is less. Beyond this point volume starts to increase; lateral cracks opening becomes so large that effect of axial compression is overcome. Early researchers believed this point of minimum volume as onset of global failure. This is where cracking becomes unstable and collapse is endemic. At the ends of specimen a triaxially confined region is developed due to end platen restraint. For specimen with height to diameter ratio less than 2 this effect is dominant. For ratio greater than 2 this effect is less. For such specimen the specimen can fail along inclined shear crack (high end friction) or through tensile splitting both (vanMier, 1998).

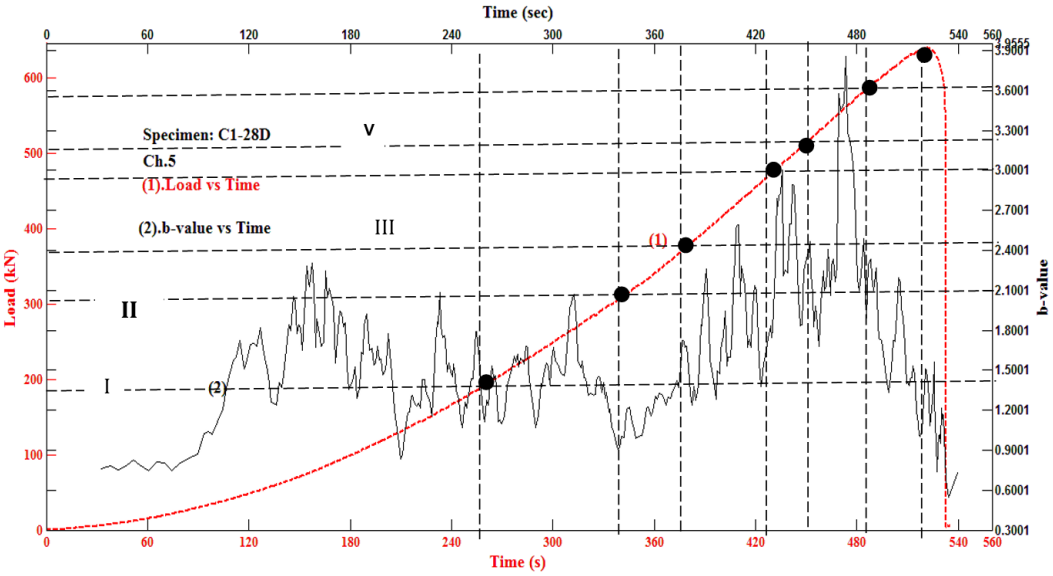

Fig. 8. AE based *b*-value variation with uniaxial compression load (Specimen; C1-29D, Ch-5).

The presence of sudden decrease in variation in *b*-value is because of the cracks had started to develop. There could be higher amplitude events in less number occurred. From stage 1 to stage-II, AE based *b*-value started to decrease due to high amplitude events occurred at the end of that stage-I, inelastic volume change begins due to the formation of a large number of new micro-cracks. At around 80% of σ_f, the test specimen's volume

is minimum (vanMier, 1998). In other words, the sum of axial stains and lateral strain will decrease. It is observed that at ~80% of σ_f, *b*-value decreasing sharply to 1.15. With further increase is stress, the *b*-value increased slightly, marking the transition from 'formation' to 'growth' stage of the newly formed cracks. After 80-90% of σ_f, the test specimen dilated and the lateral cracks has become large that the specimen's volume started to increase. Then it was followed by the onset of unstable cracking as a result of which the *b*-value decreased until the stress reached a value of 98% failure stress. The coalescence of cracks commenced at this stage. Then the b-value began to decrease sharply due to crack coalescence and the accompanying stress relief, and at the final failure they had fallen to as low. The newly formed cracks began to grow stably in number and size and the *b*-value is decreased further until 100 % failure stress. The various stages of compressive fracture and the corresponding *b*-values are summarized in Table 2. Fig. 9 shows the variation of AE based *b*-value at different curing days. It can be observed that the 'sudden decrease' occurred in *b*-value at different percentage of peak compressive stress (σ_f). By the chosen displacement rate as shown in Table-1, the specimen failed in a brittle manner, where the linear branch extends over almost the entire duration of the test.

Table 2. Various stages of compression fracture process and corresponding b-values.

Stage	Stress range	Compression fracture process	AE based *b*-value
I	0-30% σ_f	Due to short term loading the micro cracks present in ITZ are undisturbed.	1.4
II	30-50% σ_f	Micro cracks starts appear in the ITZ, cement-matrix cracking negligible	1.2
III	50-75% σ_f		
	50-60% σ_f	Micro cracks begin to form in the cement matrix The crack system becomes unstable in ITZ.	1.3
	60-75% σ_f	Cracks in ITZ becomes unstable, proliferation and propagation of cracks in cement matrix increases	1.7
IV	75-80% σ_f	Release of strain energy reach critical state and cracks becomes unstable. The stress level equals and greater than 75% σ_f is called critical stress.	1.7
V	80-90% σ_f	Volume of the specimen becomes minimum, onset of global failure of a test specimen	1.5
VI	90-100% σ_f	Stress remains constant and strain starts increasing	0.6

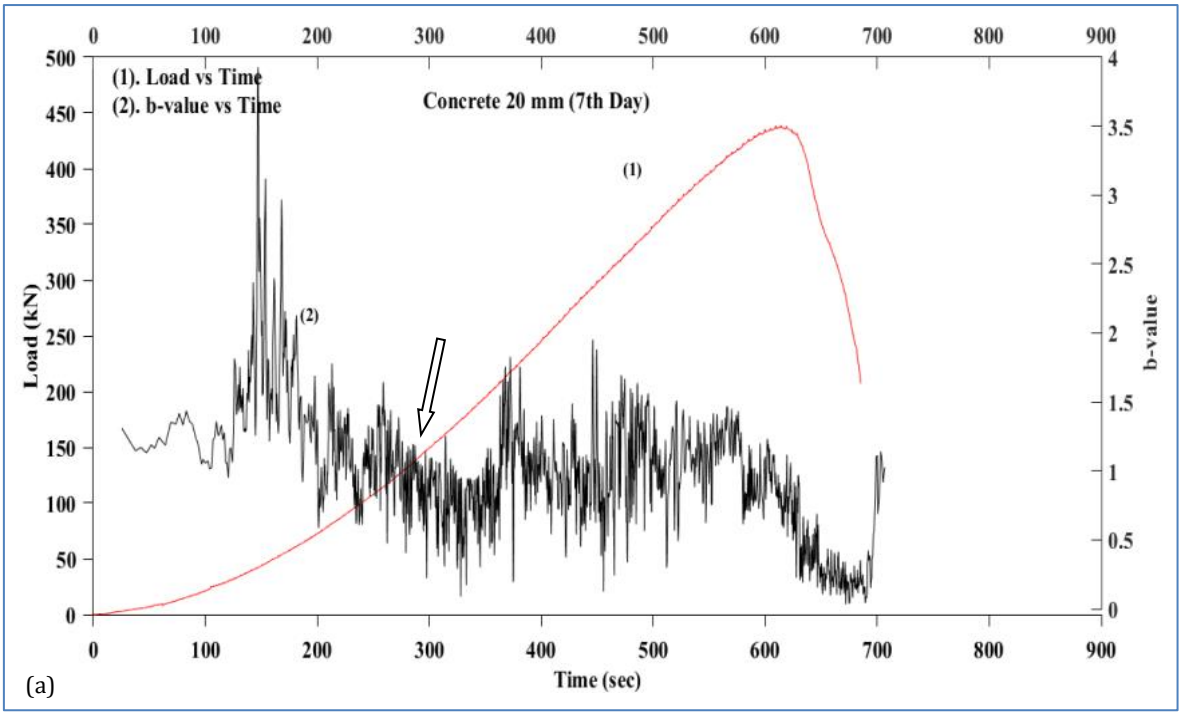

(a)

Fig. 9. (continued)

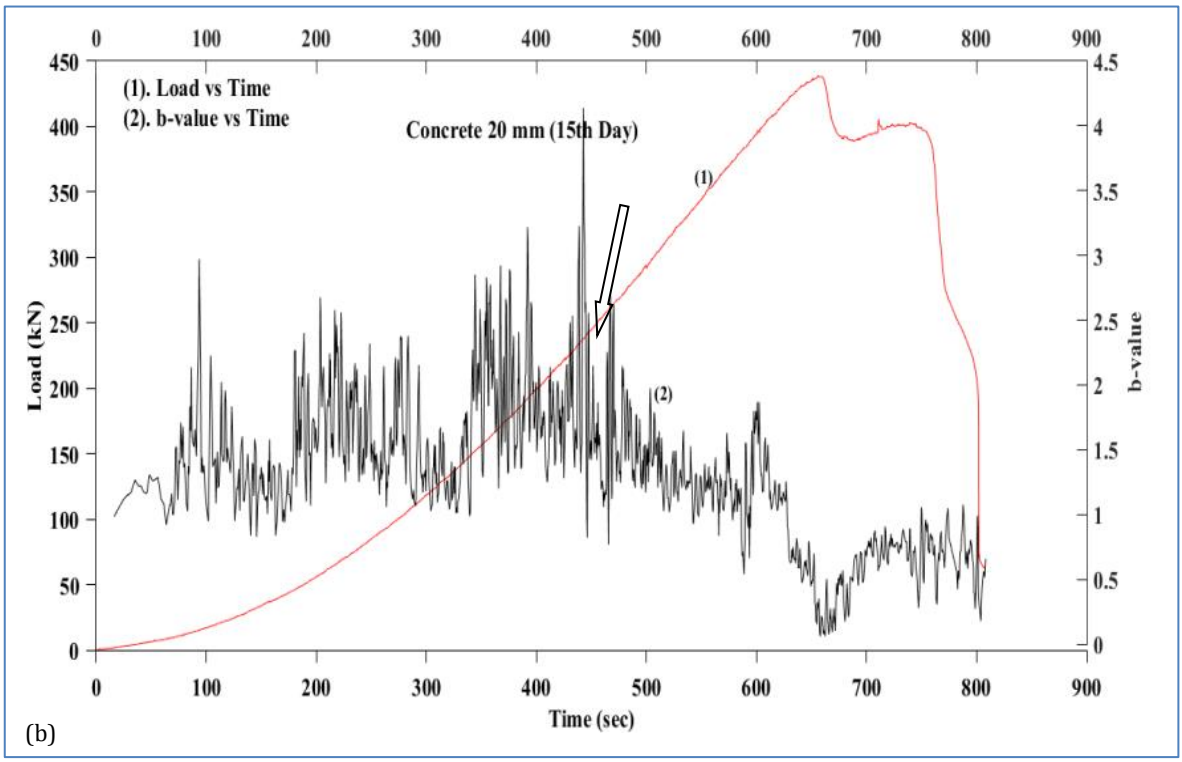

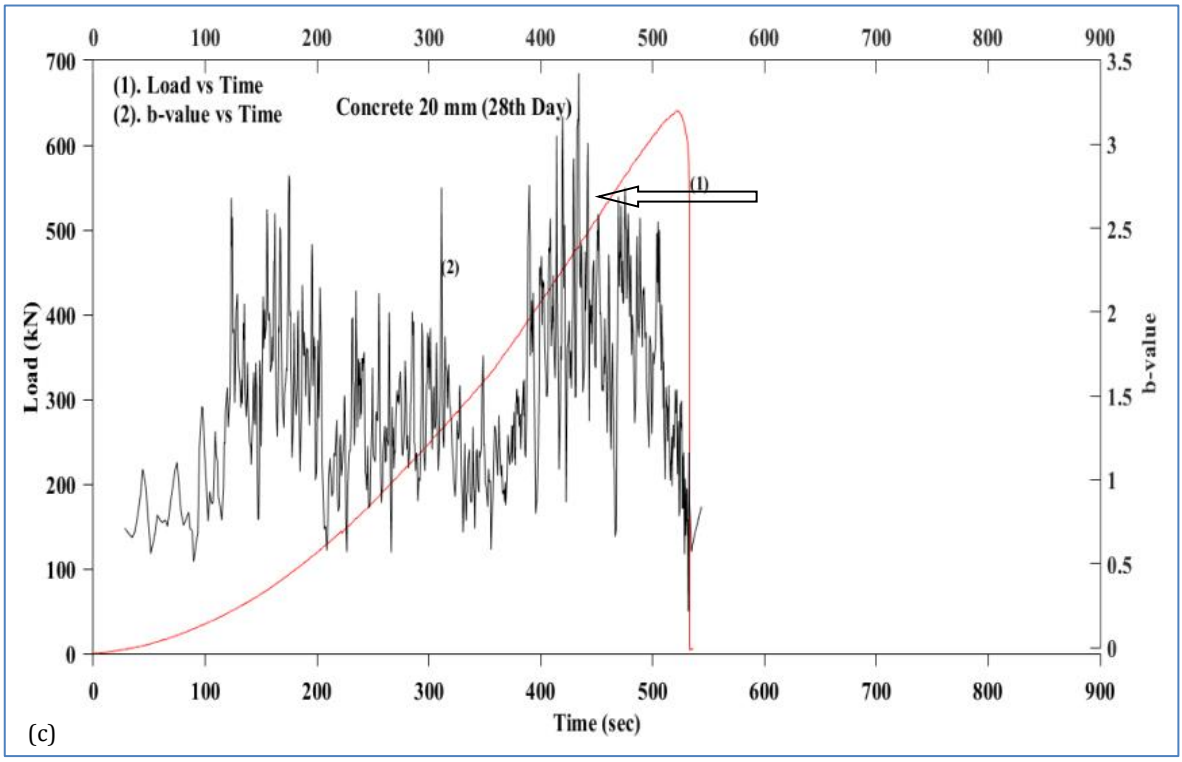

Fig. 9. AE based *b*-value variation with time at age: (a) 7 days; (b) 15 days; (c) 28 days [Concrete-I specimen] (*b*-value was computed for the total AE data recorded by both channels).

Fig. 10 shows the variation of *b*-value with time. The *b*-values were computed at curing periods of 7 days, 15 days and 28 days respectively. It is observed that *b*-values are low for concrete-I at age of 28 days, when compared with *b*-values of concrete with 7 days age. It can be observed from Fig. 3, that the compressive strengths (cylinder) range varies from 18 MPa to 22 MPa for cement mortar, 21 MPa to 25 MPa for concrete-II and 23 MPa to 29 MPa for concrete-I. The rather high variability in compressive strengths may have been due to variations in the concrete mixture proportions. Therefore, as the strength of the concrete is increasing high amplitude AE events are occurred. The number of high amplitudes events are less, hence the AE based *b*- values is low.

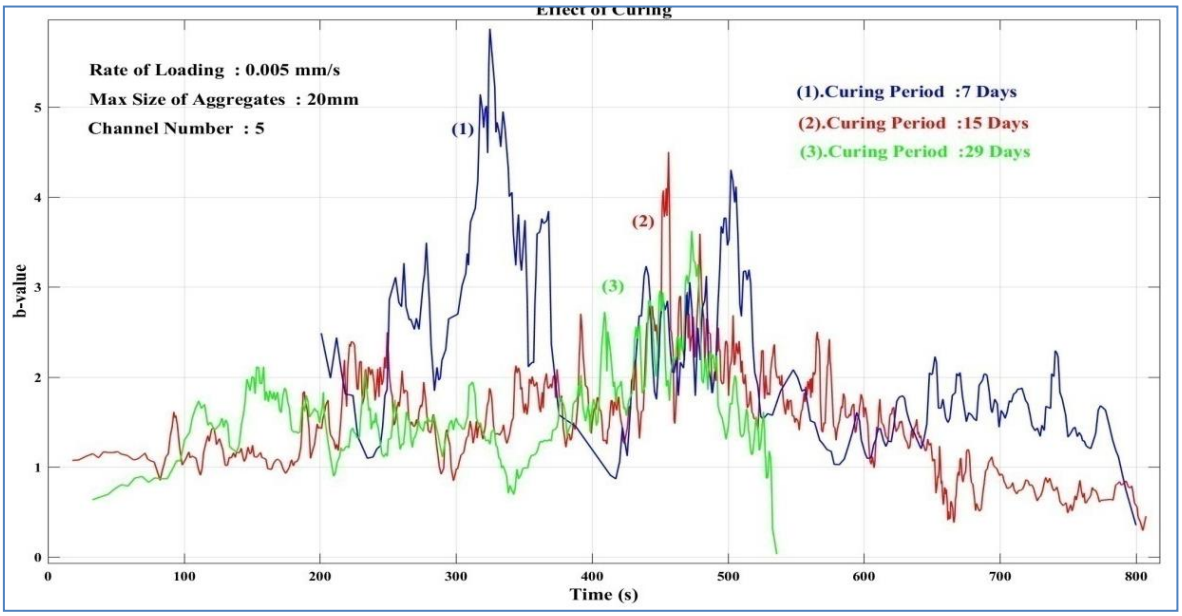

Fig. 10. Influence of curing period on AE based b-value.

6.2. Variation of AE based b-value with sensor location

It is observed that *b*-value is varying from channel to channel as shown in Fig. 11. This is due to different mechanisms or different degrees of deterioration present in the different zones or locations in the test specimen. The zone or area with the most advanced deterioration to have the lowest *b*-values.

6.3. Influence of loading rate on AE based b-value related to uniaxial compression of cementitious materials

From Fig.12 it is observed that the AE *b*-values are low for the specimen tested with high rate of loading. This may be due to release of high amplitude AE events. Higher AE activity such as large number of AE events per time and higher intensity events are observed around the peak load. These observations further prove that the instance of damage initiation is predicted by the lowest *b*-value. Low *b*-value may be due to initiation of microcracks and cracks opening. Rate of loading can accelerate the micro crack damage which is accompanied by the release of AE. If the rate of loading is too fast (more than what is suggested by the ASTM), there can be a surge or heavy rush of AE. The fluctuations in the *b*-value variation is more when the rate of loading is high.

AE signals experience attenuation during fracture process in concrete structures, and for that matter in any other imperfect or quasi-brittle materials. Attenuation of AE may be due to heterogeneity of the material as well as micro cracking. A change in the volume of the specimen causes a change in the propagation path length from the crack to the AE sensor, which may affect the recorded AE amplitude. Both the AE amplitude and AE energy as well as the number of AE would be affected uniformly be it weak or strong. In this present study authors invariably use the number as well as AE amplitude for computing the *b*-value. Therefore, it should not an issue since both low amplitude and high amplitude of AE are considered to study the fracture process.

When the loading rate is faster, quick cracking development lead to sudden fluctuations in the *b*-value at higher loads. Since the concrete behaves relatively more brittle at higher loading rates (or at higher strain rates), the *b*-values are lower in an average as a few and stronger cracking AE events are created, in contrast to more and weaker cracking events for low rate of loading.

6.4. Influence of coarse aggregate size on released AE

Fig. 13 shows the variation of AE based *b*-value with time for concrete-II and cement mortar specimens cured for 28 days. When compared *b*-values of concrete with mortar, low *b*-values are observed forconcrete. The reason could be during fracture process in concrete, high amplitude events in less number are released. A decrease in *b*-value is seen due to material damage (micro-cracking and macro-cracking) while *b*-value show a rising trend due to toughening mechanisms like coarse aggregate interlocking, tortuosity of crack path. It is known that AE events are related to cracking. These events are recorded by PZT sensors as electrical signals. And these signals are decayed sinusoidal waves by nature. The number of cycles occurring in unit time in the signal is known as frequency of AE. The "frequency range of the source event" is dependent on its "event duration" (inverse relationship). That is, the source event has a 'broadband spectrum' extending upwards from zero frequency, and starting to decline at a frequency that is inversely proportional to its time duration. This source event duration (t_{ed}) is different from the resulting signal duration (t_{sd}). During fracture process t_{ed} could be different in cement mortar compared with concrete.

Source event duration (t_{ed}) could be on the order of ($\frac{X}{V_{cr}}$) where 'X' is the distance moved by the crack and 'V_{cr}' the velocity with which crack is moving. In case of cementitious materials, cracks propagate at several meters per second, giving ample spectral content up from zero and up through the ordinary AE frequency range. The documented cases for the velocities of fast-running cracks are generally for metals, glass (Pollock, 1981). But given the nature of the stiff and brittle constituent materials (or coarse aggregates), velocities on this same order would be the case for cracks in concrete also. To illustrate this, curves of cumulative hits versus AE energy during the compressive fracture process are shown in Fig. 14a – Fig. 14c respectively.

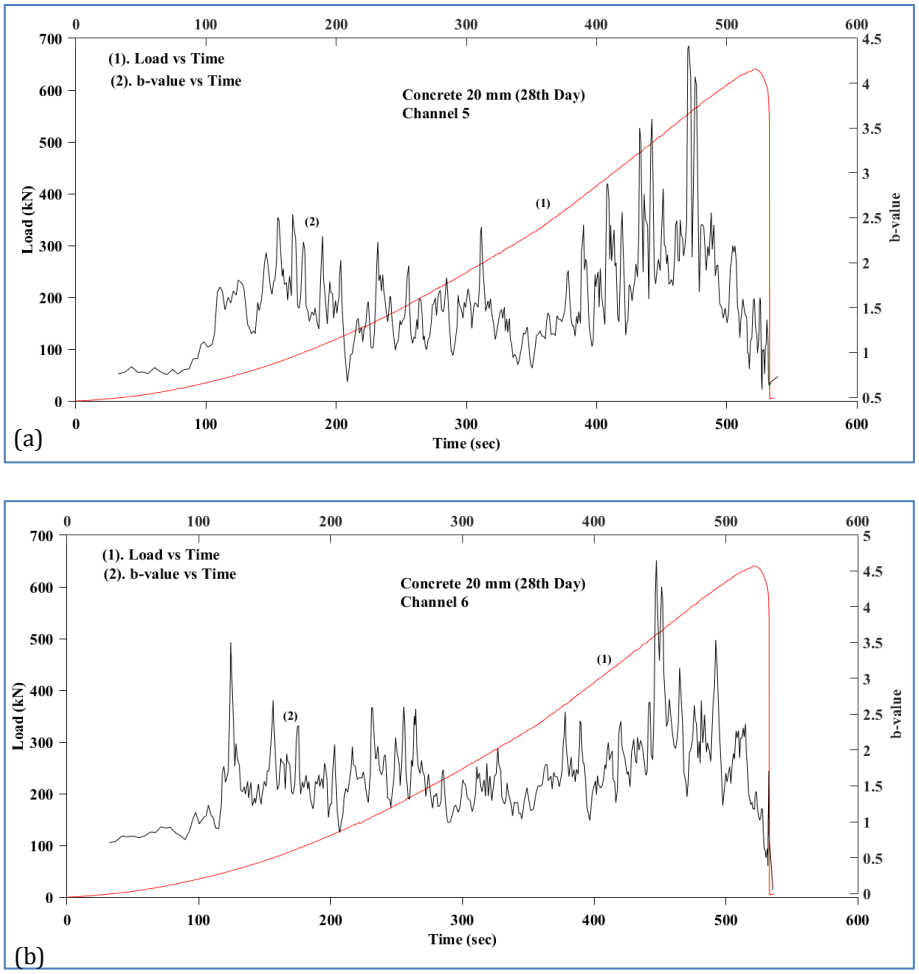

Fig. 11. Variation in AE based *b*-value with time and load: (a) Ch-5; (b) Ch-6.

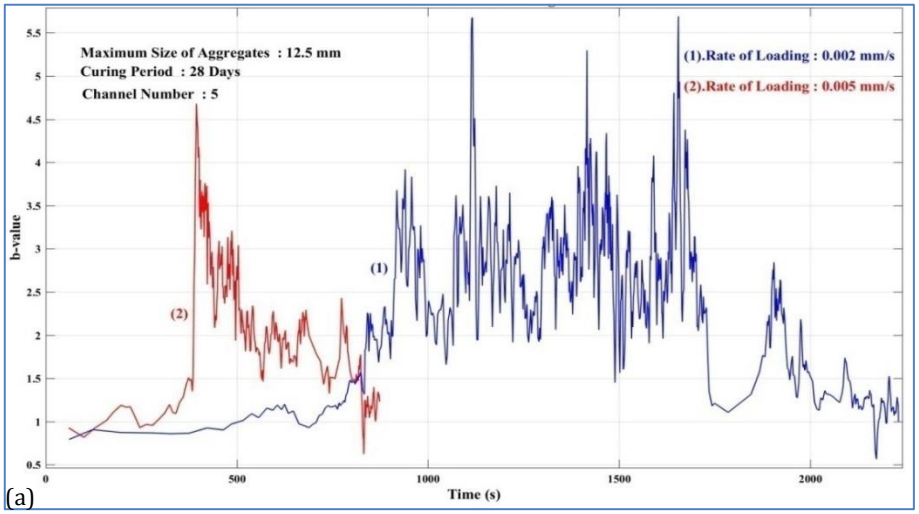

Fig. 12. (continued)

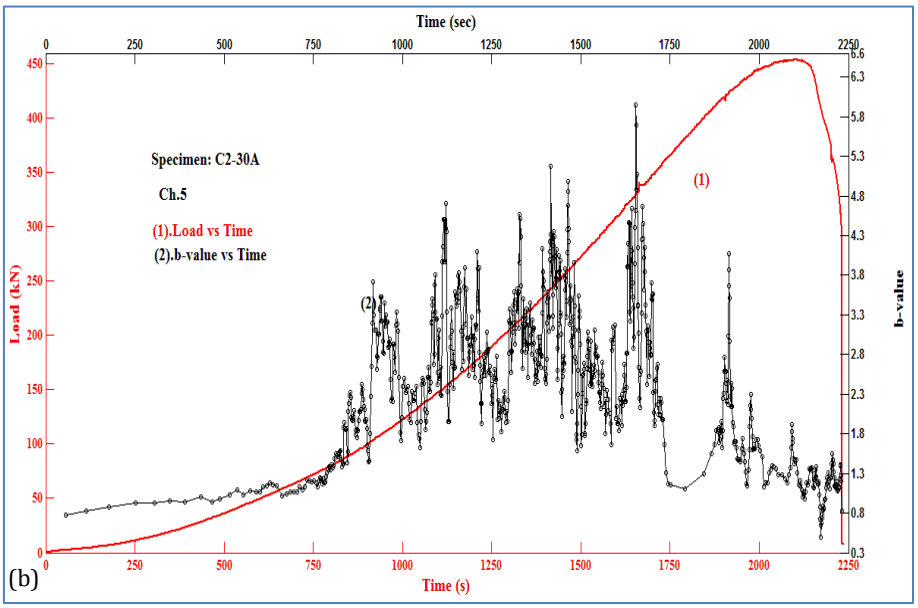

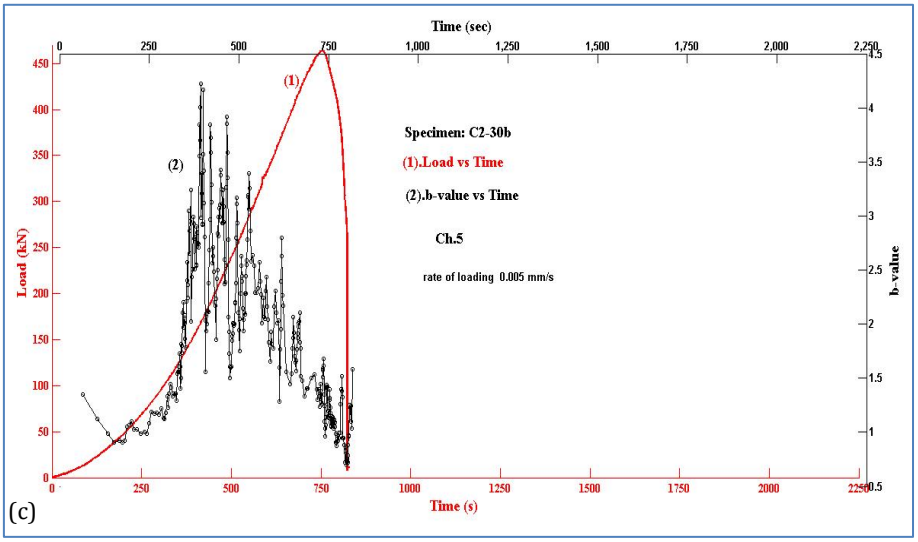

Fig. 12. Influence of loading rate on:
(a) AE based *b*-value; (b) Specimen tested with 0.002 mm/s (c) specimen tested with 0.005 mm/s.

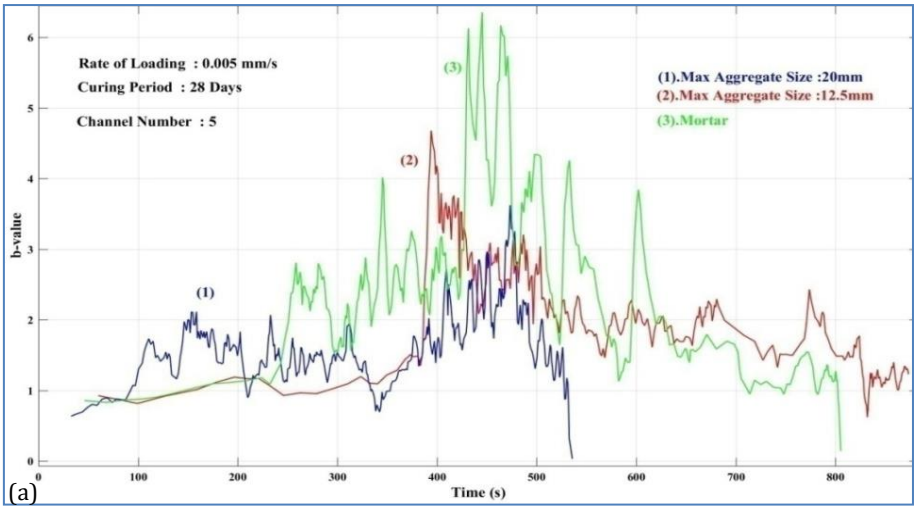

Fig. 13. (continued)

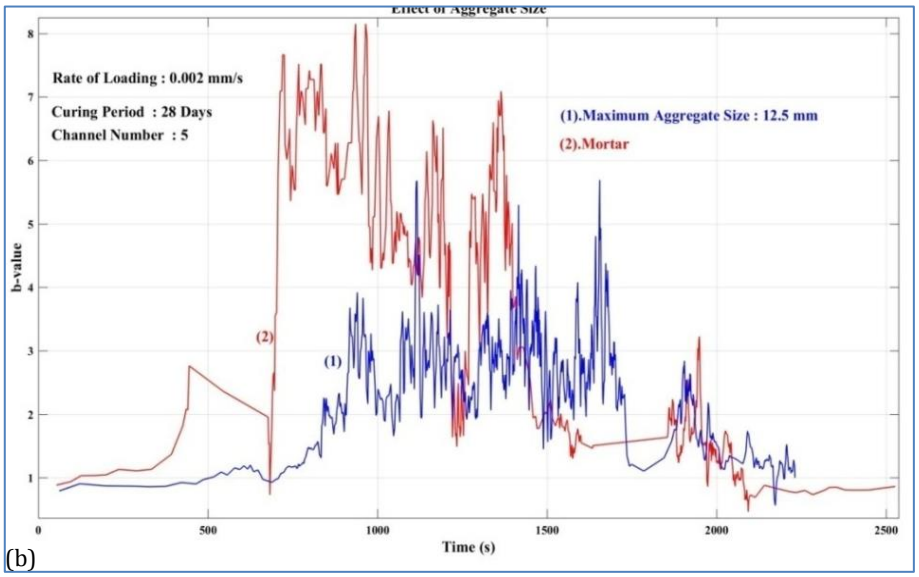

Fig. 13. AE based *b*-value variation in: (a) concrete-I and mortar; (b) concrete-II and mortar.

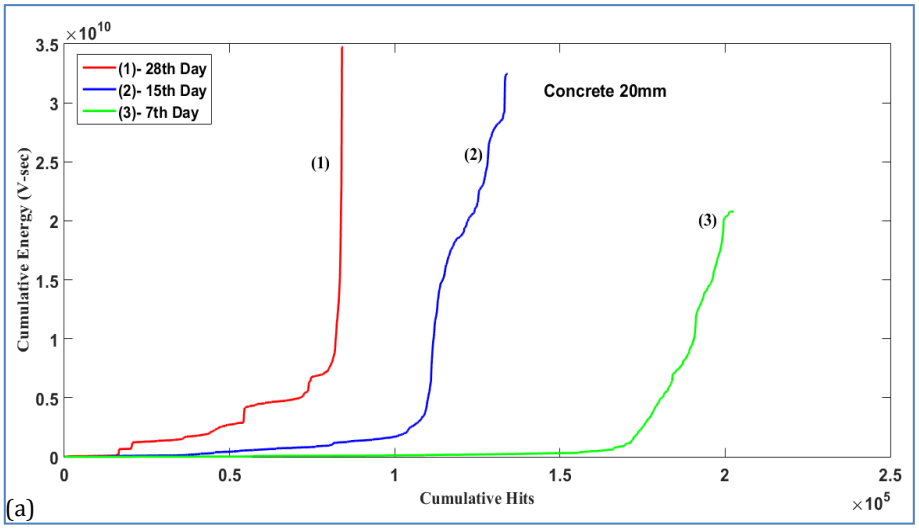

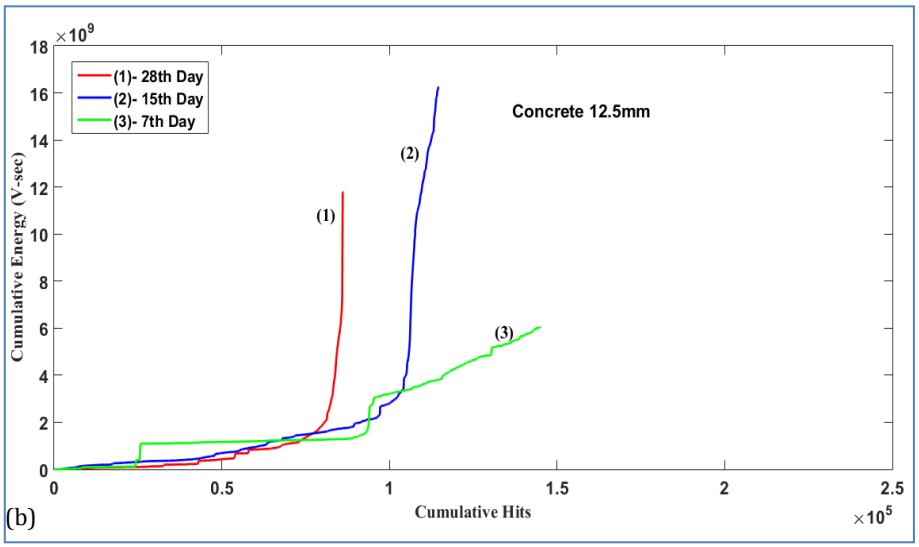

Fig. 14. (continued)

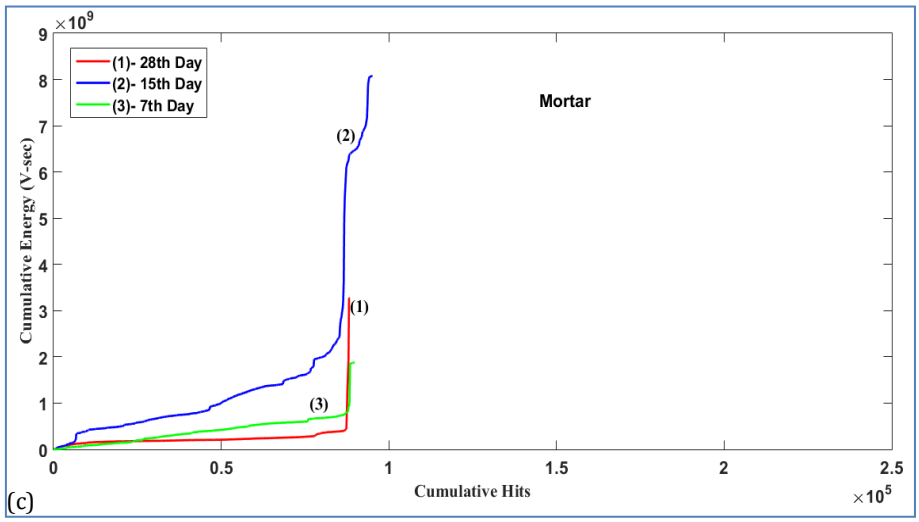

Fig. 14. Variation of AE hits released under uniaxial compressive load: (a) Concrete-I; (b) Concrete-II; (c) cement mortar.

From Fig. 14, it is observed that the number of AE hits recorded is different in the three cementitious materials. The energy released also different. As the toughness of the material is increasing the energy released is decreased. Because the coarse aggregate size in concrete might influence the AE released as shown in Fig. 14. The fracture process of coarse aggregate might be different from cement matrix cracking because of the higher compressive strength and homogeneity of the aggregate.

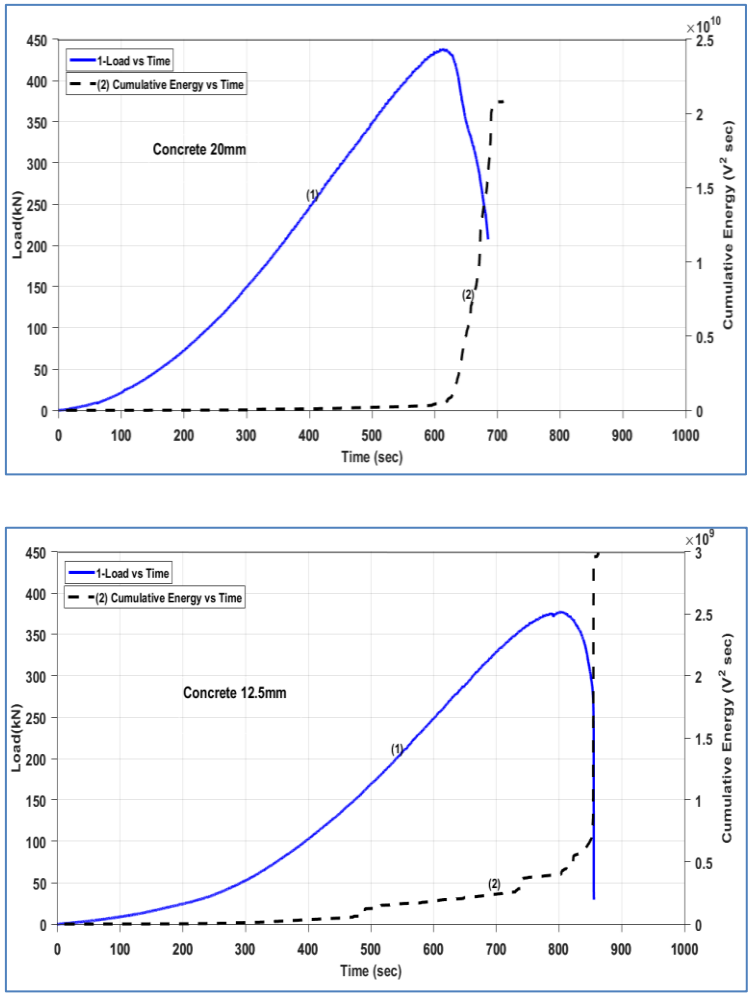

Fig. 15. (continued)

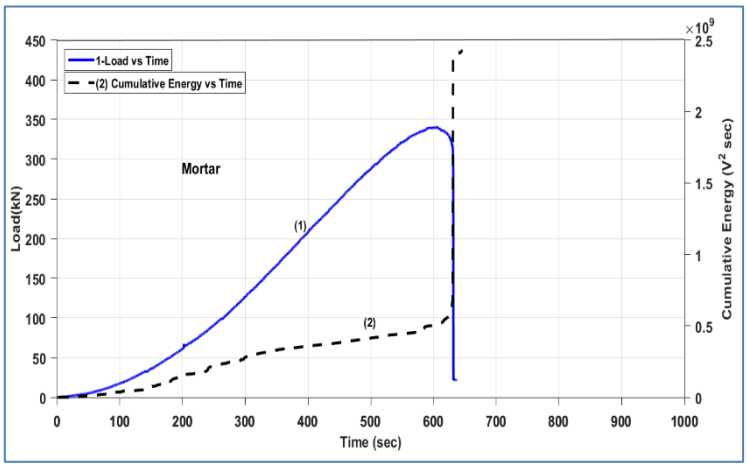

Fig. 15. Variation of AE cumulative energy released with uniaxial compressive load: (a) Concrete-I; (b) Concrete-II; (c) cement mortar.

Fig. 15, shows the AE energy released during the compressive fracture process in the three different cementitious materials. First observation is a very small AE activity occurs before peak load. From Fig. 15, one can observe that the jump in AE energy release occurs at or near peak load in Concrete-I. It indicates the onset of critical crack growth. Second observation is, AE energy release rate (the slope of the cumulative AE energy plots of Fig. 15) is greatest at the peak load, perhaps indicating that the strain energy released is maximum at this point. Also there is a taper in the AE energy release rate that occurs at before the pre-peak. While the mortar exhibits less, it is very evident in both in concrete-I and concrete-II specimens. Perhaps this suggests that the AE source mechanisms are different between the mortar and the concretes in the pre-peak region (Landis and Baillon, 2002). The reason might include the mobilization of friction, bridging, and other energy dissipation mechanisms in cementitious materials. When observed the 'AE frequency spectrum' as opposed to the 'AE source spectrum', the effects of attenuation come into it. The frequency spectrum of an electrical signal is the distribution of the amplitudes and phases of each frequency component against frequency. AE are the transient elastic waves within a material, caused by the release of localized strain energy. An event source is the phenomenon which releases elastic energy into the material, which then propagates as an elastic wave. The spectrum of the "AE wave energy" change as it propagates, with 'material absorption', away from the source. This will certainly be important when it comes to working up procedures for using AE testing on large concrete structures in-situ. Because it assumes that the frequency (f) dependent attenuation will be due to material absorption and thus proportional to AE signal frequency (f). Considering the inhomogeneity of cementitious material (aggregate-related), that this proportionality relationship will apply. Rayleigh scattering may also come into it at higher frequencies. The relationship between attenuation coefficient and frequency is likely to be different depending on whether the wavelength (λ) is greater than or less than the coarse aggregate size. The relation between wave frequency and velocity is given in Eq. (2).

$$V = f\lambda\,. \tag{2}$$

In Eq. (2), V is the velocity, f is frequency and λ is wave length. Generally AE due to fracture process in cementitious materials is in the range of 100 kHz to 1000 kHz (Landis and Baillon, 2002). For a typical AE velocity in concrete of 4,100 m/s, a wavelength of 20 mm would correspond to a frequency of 205 kHz, which is within the frequency ranges of AE signals in concrete. For a frequency range of 100–500 kHz, the corresponding wavelengths are 40 mm–8 mm, respectively. Thus both concrete-II (coarse aggregate size 12.5 mm] and concrete-I (coarse aggregate size 20 mm) have aggregates in this regime of ultrasonic scattering. This ultrasonic scattering causes additional signal attenuation. Also material absorption takes place. Therefore reduce the total elastic wave energy that reaches the AE sensors. Due to the attenuation of AE reaching the AE sensor will be different in cementitious materials. Because, when compared with concrete-I, the coarse aggregate size is different in concrete-II and cement mortar. Hence the material absorption of the AE is different. Therefore the release of AE energy is different as shown in Fig. 15.

7. Conclusions

Based on the above experimental results, the given below major conclusions can be drawn:

- Determination of b-value using the G-R relationship is useful to study the fracture process in cementitious materials. The AE based b-value is closely related to the formation and propagation of cracks in the damage process of concrete and it decreases rapidly before the test specimen is reaching to peak load.
- AE based b-value at stresses close to failure clearly indicated the onset of 'unstable cracking' as well as 'crack coalescence' leading to dynamic failure of the cementitious materials.
- Since the AE peak amplitudes influences AE based b-value, it will be useful to examine the link between attenuation, propagation distance, frequency of sensor and b-value. Such an attempt is required for the studies on cementitious materials.

- When the compression toughness of the cementitious material increases, higher *b*-values are observed.
- Quick cracking occurred and lower *b*-values were observed, when the loading rate is high.
- As the coarse aggregate size in the cementitious material increases, the cumulative AE energy is higher. This may be due to toughness of the cementitious material.

The present study, is related to the influence of the coarse aggregate size in cementitious materials on AE peak amplitude distribution. Although water/cement ratio and cement quantity are different in the mixtures, the present study is limited to only coarse aggregate size influence of AE based *b*-value. Future work should investigate the variation of AE based *b*-value for changes in toughness and ductility of cementitious materials under uniaxial compression.

Appendix A.

A.1. *Gutenberg-Richter (G-R) empirical relation*

It is known from the principles of seismology that the earthquake events of larger magnitude occur less frequently than the events of smaller magnitude. This observation in seismology is known as the Gutenberg-Richter (G-R) law (Gutenberg and Richter, 1954).

$$\log_{10}\mathrm{N(M)} = \mathrm{a} - \mathrm{bM}\,. \tag{A1}$$

G-R law given in Eq. (A1) is an empirical relation between the magnitude and total number of earthquakes occurred in a given region during a specific time interval. G-R law represents the cumulative distribution function (CDF) of seismic events using a frequency-magnitude relation. In Eq. (A1), *M* is the Richter magnitude of earthquakes. It is the logarithm of the integral of slip along the fault during an earthquake. *N(M)* is the total number of earthquakes of magnitude greater than M.

$$\mathrm{N(M)} = \int_{\mathrm{M}}^{\infty} \mathrm{n(M)dM}\,. \tag{A2}$$

In other words, *N(M)* is the number of earthquake events having a magnitude *M* occurred during a specific time interval in a particular region. 'a' and 'b' are empirical constants. The constant 'a' is dependent on the seismicity rate which varies from region to region. The constant 'b' is the *b*-value. In fact, *b*-value is the slope of the amplitude CDF. In Eq. (A1), the *b*-value is the negative gradient of the log-linear plot of earthquake occurrences and the corresponding magnitudes. In Eq. (A2), *n(M)* is the number of earthquakes of magnitude *M. N(M)* can be found by integrating *n(M)* with respect to M over a range of *M* to ∞.

A.2. *Analogy between earthquake occurrences and acoustic emissions released during fracture in solids*

Similar to the occurrence of earthquakes, during fracture process in solids, higher amplitude AE events occur less in number, and lower amplitude AE events occur more in number. Researchers implemented G-R law to the AE peak amplitude distribution data to study the scaling of AE.

A.3. *Decibel*

Generally, decibel (dB) describes a ratio. The dB is a logarithmic way of describing a ratio. If the ratio is related to voltage

$$\mathrm{dB} = 10\log_{10}\left[\frac{\mathrm{v_p}}{\mathrm{v_{ref}}}\right]^2, \tag{A3}$$

where V_p is the peak signal voltage in micro-volts refereed to the pre-amplifier input. In general, $(\mathrm{dB})_{\mathrm{AE}}$ is used for measurement of AE signal peak amplitude A. From Eq. (A3) AE peak amplitude in decibels can be written as

$$\mathrm{A_{dB}} = 10\,log_{10}\left[\frac{\mathrm{A_{max}}}{\mathrm{A_{ref}}}\right]^2, \tag{A4}$$

$$\mathrm{A_{dB}} = 20log_{10}\left[\frac{\mathrm{A_{max}}}{\mathrm{A_{ref}}}\right]. \tag{A5}$$

A.4. *Earthquake magnitude and amplitude*

From Eq. (A1) one can write

$$M = \frac{\mathrm{a}-(log_{10}\mathrm{N})}{\mathrm{b}}. \tag{A6}$$

From Eq. (A6) and Eq. (A2), it can be observed that the earthquake magnitude is proportional to the logarithm of the maximum amplitude. Because Richter magnitude scale assigns a magnitude number to quantify the size of an earthquake. Therefore earthquake magnitude *(M)* is determined by measuring the amplitude of the largest wave (A_{max}) recorded on the seismogram. Hence

$$\mathrm{M} \propto \frac{2}{3}\mathrm{c}\log_{10}\mathrm{A_{max}}\,, \tag{A7}$$

where c refers to the time constant of the transducer and the associated circuitry. Substituting Eq. (A7) into Eq. (A1). Here earthquake magnitude *M* is analogous to AE signal peak amplitude, A_{max}. AE magnitude, which has no units is computed using the amplitude data (units: dB or volts).

$$\log_{10}\mathrm{N(M)} = \mathrm{a} - \mathrm{b_{AE}}[20\log_{10}\mathrm{A_{max}}] \quad [A_{ref}=1]\,. \tag{A8}$$

A.5. *Comparison of M and amplitude of AE event*

Comparing M values both in case of earthquake phenomenon and acoustic emission phenomenon.

In case of earthquakes, M value for Eq. (A1) is given in Eq. (A7). In case of acoustic emission: M value is given in Eq. (A8).

From Eq. (A1) and Eq. (A8).

$$20\,\mathrm{b_{AE}}\log_{10}\mathrm{A_{max}} = \mathrm{b}\frac{2}{3}\mathrm{c}\log_{10}\mathrm{A_{max}}\,, \tag{A9}$$

Considering AE transducer is a velocity transducer (Colombo et al., 2003) and assuming 'c' is equal to 1.5. Eq. (A9) becomes

$$20b_{AE} = b\frac{2}{3}c\,, \tag{A10}$$

$$b_{AE} = \frac{b}{20}\,, \tag{A11}$$

$$\log_{10}N(A) = a - b_{AE}[A_{dB}]\,. \tag{A12}$$

Therefore, G-R law given in Eq. (A1) is modified to implement for AE testing is given below.

$$\log_{10}N(A) = a - b\left[\frac{A_{dB}}{20}\right]. \tag{A13}$$

where A_{dB} is the peak amplitude of the AE hits (or events) in decibels. *b* is the AE-based *b*-value. *N(A)* is the number of AE hits of amplitude greater than or equal to A. 'a' is constant. The constant 'a' is determined mostly based on surrounding noise of the test area. Therefore to use the same G-R law given in Eq. (A1), one should divide acquired AE peak amplitudes by 20. Because AE peak amplitude recorded is in dB units and Richter magnitude of earthquakes defined in terms of logarithm of maximum amplitude.

REFERENCES

Carpinteri A, Lacidogna G, Pugno N (2006). Richter's laws at the laboratory scale interpreted by acoustic emission. *Magazine of Concrete Research*, 58(9), 619-625.

Colombo IS, Main IG, Forde MC (2003). Assessing damage of reinforced concrete beam using *b*-value analysis of Acoustic emission signals. *Journal of Materials in Civil Engineering*, 15(3), 280-286.

Grosse C, Ohtsu M (2008). Acoustic Emission Testing. Berlin, Springer-Verlag., Heidelberg:

Gutenberg B, Richter CF (1954). In Seismicity of the Earth and Associated Phenomena, Princeton University Press, Princeton, NJ, USA, 2nd Ed.

Holford KM (2000). Acoustic emission - Basic principles and future directions. *Strain*, 36(2), 51-54,

Ko W, Yu C (2009). Application of Gutenberg Richter Relation in AE Data Processing. *International Journal of Applied Science and Engineering*, 7(1), 69-78.

Kalyanasundaram P, Mukhopadhyay CK, SubbaRao SV (2007). Practical acoustic emission. Narosa Publishing House private limited, New Delhi.

Kurz JH, Finck F, Grosse CU, Reinhardt HW (2006) Stress drop and stress redistribution in concrete quantified over time by the *b*-value analysis. *Structural Health Monitoring*, 5, 69–81.

Landis EN, Baillon L (2002). Experiments to Relate Acoustic Emission Energy to Fracture Energy of Concrete. *Engineering Mechanics*, 128(6), 698-702.

Mogi K (1962) Magnitude–frequency relation for elastic shocks accompanying fracture of various materials and some related problems in earthquakes. *Bulletin of Earthquake Research Institute, Tokyo University*, 40, 831–853.

Mehta PK, Monteiro PJM (2006) Concrete: Microstructure, properties and materials. McGraw-Hill, Third edition.

Nair A, Cai C (2010). Acoustic emission monitoring of bridges: Review and case studies. *Engineering Structures*, 32(6), 1704-1714.

Neville AM (2011). Properties of Concrete. Pearson Education Limited, Edinburgh Gate Harlow Essex CM20 2JE England.

Ohtsu M (1998). Basics of acoustic emission and applications to concrete engineering, *Materials Science and Research International*, 4(3)131-140.

Pollock AA (1981). Acoustic emission amplitude distributions. *International Advances in Nondestructive Testing*, 7, 215-239.

Datt P, Kapil JC, Kumar A (2015). Acoustic emission characteristics and *b*-value estimate in relation to waveform analysis for damage response of snow. *Cold Regions Science and Technology,* 117, 170-182.

Rao MVMS, Prasanna Lakshmi KJ (2005). Analysis of *b*- value and improved *b*-value of acoustic emissions accompanying rock fracture. *Current Sci*ence, 89, 1577-1582.

RILEM TC 212-ACD (2010a). Acoustic emission and related NDE techniques for crack detection and damage evaluation in concrete. Measurement method for acoustic emission signals in concrete. *Materials and Structures,* 43(9), 1177-1181.

RILEM TC 212-ACD (2010b). Acoustic emission and related NDE techniques for crack detection and damage evaluation in concrete. Test Method for damage qualification of reinforced concrete beams by AE. *Materials and Structures,* 43(9), 1183-1186.

RILEM TC 212-ACD (2010c) Acoustic emission and related NDE techniques for crack detection and damage evaluation in concrete. Test method for classification of active cracks in concrete structures by acoustic emission. *Materials and Structures,* 43(9), 1187–1189.

Proverbio E (2011). Evaluation of deterioration in reinforced concrete structures by AE technique. *Materials and Corrosion*, 62(2), 161-169.

Schumacher T, Higgins CC, Lovejoy SC (2011). Estimating operating load conditions on reinforced concrete highway bridges with b-value analysis from acoustic emission monitoring. *Structural Health Monitoring*, 10(1), 17-32.

Shiotani T, Yuyama S, Li Z, Ohtsu M (2001). Application of AE improved *b*-value to quantitative evaluation of fracture process in concrete materials. *Journal of Acoustic Emission.*

User's Manual. AE ^{win} SAMOS Software (2004). Physical Acoustics Corporation, Princton Jct, NJ, USA.

Uchida, M, Okamoto T, Ohtsu M (2011). Damage of reinforced concrete qualified by AE. *Challenge Journal of Concrete Research Letters*, 2(3), 286-289.

vanMier JGM (1997). Fracture Process of Concrete. Assessment of material parameters for fracture models. CRC Press.

vanMier JGM (1998). Failure of concrete under uniaxial compression: An overview. *Proceedings of the 3rd International conference on Fracture mechanics of concrete and concrete structures (FraMCoS-3)*, Gifu, Japan, AEDIFICATIO, Freiburg, Germany, 1169-1182.

Vidya Sagar R, Rao MVMS (2014). An experimental study on loading rate effect on acoustic emission based b-values related to reinforced concrete fracture. *Construction and Building Materials*, 70, 460-472.